Global compilation of interferometric synthetic aperture radar earthquake source models:
1. Comparisons with seismic catalogs

J. Weston,[1] A. M. G. Ferreira,[1,2] and G. J. Funning[3]

[1]   While many earthquakes have now been studied using interferometric synthetic aperture radar (InSAR) data, a full assessment of the quality and additional value of InSAR source parameters compared to seismological techniques is still lacking. We compile a catalog of source models obtained using InSAR and estimate the corresponding centroid moment tensor (CMT) parameters; we refer to this compilation as the ICMT archive. We compare source parameters from over 70 InSAR studies of 57 global earthquakes with those in the Global CMT (GCMT), International Seismological Centre (ISC) and Engdahl-Hilst-Buland (EHB) seismic catalogs. We find an overall good agreement between fault strike, dip and rake values in the GCMT and ICMT archives. Likewise, the differences in seismic moment between these two archives are relatively small, and we do not find support for previously suggested trends of InSAR leading to larger moments than seismic data. However, epicentral locations show substantial discrepancies, which are larger for the GCMT (median differences of ~21 km) than for the EHB and ISC catalogs (median differences of ~10 km). Since InSAR data have a high spatial resolution, and thus should map epicentral locations accurately, this allows us to obtain a first independent estimate of epicentral location errors in the seismic catalogs. Earthquake depths from InSAR are systematically shallower than those in the EHB catalog, with a median of differences of ~5 km. While this trend may be partly due to unmodeled crustal complexity, it is also compatible with the observation that the rupture of crustal earthquakes tends to propagate upward in the seismogenic layer.

1.   Introduction

[2]   The launch of the European Space Agency satellite ERS-1 in 1991 heralded the beginning of an era of global coverage of synthetic aperture radar (SAR) observations. As geodesists learned how to exploit this data source and additional SAR satellites were launched by multiple agencies, an alternative, nonseismological, method for the study of shallow earthquakes was established.

[3]   The phase of a radar signal is a function of the distance between the radar antenna (in this case, the satellite) and the radar target (in this case, the ground). Therefore, by differencing the phase of SAR images acquired at different times we can in principle detect changes in that distance that are due to the movement of the ground toward or away from the satellite between acquisitions. If one SAR image is acquired before, and another after, an earthquake, a fine resolution map of the surface deformation due to that earthquake can be generated. This technique is known as interferometric SAR (InSAR). Elastic dislocation modeling of the surface displacements measured by InSAR can then be used to estimate the source parameters of the earthquake, independent of any information from seismology (for a review, see, e.g., *Feigl* [2002]).

[4]   Since the breakthrough study of the 1992 Landers earthquake [*Massonnet et al.*, 1994], over 60 earthquakes have been studied with InSAR, spanning a range of magnitudes from 4.4 to 8.5. The number of events is such that it is now possible to make statistically significant comparisons between source parameters obtained by analysis of InSAR data and those derived from teleseismic data. This study, along with the companion study by *Ferreira et al.* [2011], is the first attempt to make such a comprehensive comparison. For each event that we consider, one or more centroid moment tensors (CMTs) are calculated from published InSAR earthquake studies, and compared to equivalent seismic information.

[5]   Various organizations routinely report earthquake source parameters shortly after an earthquake. For example, the

[1]School of Environmental Sciences, University of East Anglia, Norwich, UK.
[2]Also at ICIST, Instituto Superior Técnico, Technical University of Lisbon, Lisbon, Portugal.
[3]Department of Earth Sciences, University of California, Riverside, California, USA.

Global CMT (GCMT) project has reported source parameters of moderate to large global earthquakes from 1976 to the present day. The GCMT method [*Dziewonski et al.*, 1981; *Dziewonski and Woodhouse*, 1983a, 1983b] uses long-period body and surface waveforms to estimate the origin time, location and depth of a centroid of stress glut along with the corresponding moment magnitude and seismic moment tensor. The magnitudes and moment tensors in the GCMT catalog are generally considered authoritative, being extensively used in a large range of applications from seismic hazard assessment to active tectonic studies. Another widely used seismic catalog is that produced by the International Seismological Center (ISC), which compiles earthquake information and body wave arrival times from over 100 organizations worldwide into a comprehensive data set [e.g., *Adams et al.* 1982]. This data set is then reprocessed and reanalyzed by the ISC, resulting in an extensive bulletin of hypocenters and phase readings of global seismicity; the total number of events listed each month in the ISC bulletin is several times greater than those obtained by any other worldwide earthquake location service. The *Engdahl et al.* [1998] (EHB) algorithm has been developed to improve hypocenter determinations made by the ISC and other organizations. Among other features, the EHB method uses traveltime tables from an improved Earth model, corrects for ellipticity and for lateral variations in crustal and upper mantle properties and uses a new statistical procedure for the inclusion of a variety of teleseismic depth phases. This method has been applied to a large number of earthquakes and has resulted in significant improvements, notably in depth determinations, which are reported in the EHB bulletin. All these catalogs represent considerable efforts by the seismological community and led to significant advances in geosciences. Nevertheless, a current limitation is that often earthquake catalogs do not report accurate uncertainties associated with earthquake parameters, which, together with the general nonexistence of ground truth solutions, makes the assessment of the quality of the catalogs very difficult. Thus, the comparisons with InSAR solutions that we carry out in this study constitute a novel, alternative approach to address these issues.

[6] One simple, yet instructive, comparison we perform is between the locations of earthquakes obtained through InSAR, and those estimated by various seismic methods. Since InSAR provides an "in situ" observation of the earthquake deformation, we should expect those locations to be the more accurate, especially in regions where seismic networks are sparse or where velocity models of the crust and upper mantle are poorly constrained. Indeed, regionally systematic patterns of mislocation of seismically estimated earthquake centroids and/or hypocenters when compared to InSAR locations may be one identifier of the effects of incorrect velocity models.

[7] Additionally, we compare the geometric parameters (strike, dip, rake) of our InSAR centroid moment tensors with their seismic counterparts, to see if these, too have systematic differences. Again, such differences can be reflective of problems with the velocity models, but may also reflect ambiguities in the InSAR studies; indeed we include models based upon multiple published studies, in order to assess the level of model-based uncertainty in those estimates.

[8] Finally, consideration of differences in seismic moment allow us to evaluate a hypothesis proposed around a decade ago, that InSAR data can routinely overestimate the "true"

seismic moment [e.g., *Wright et al.*, 1999; *Feigl*, 2002]. Such overestimates could reflect the capturing of some early postseismic deformation within coseismic interferograms. Our comparisons can cast light on whether such issues are, in general, significant.

2. InSAR CMT (ICMT) Compilation

[9] We compiled CMT source parameters (spatial centroid location, seismic moment and fault's geometry) for global earthquakes occurring since 1992 studied using InSAR from over 80 studies published in the literature. In this study we focus on the first 15 years of earthquakes studied using InSAR; thus, we use 57 earthquakes that occurred between 1992 and 2007 for which there are both GCMT and InSAR reported source parameters (see Tables 1–3). Figure 1 shows the geographical location of the earthquakes that we use. As expected, most earthquakes are located within the continents, with depths shallower than 60 km (except for the 2005 Tarapaca, Chile, earthquake, which has a GCMT depth = 97.6 km); while 18 of the earthquakes have ruptured up to the surface, the other 39 earthquakes have buried ruptures. The magnitudes of the earthquakes studied are in the range M_w 5.0–8.4, with about half of the earthquakes having magnitudes M_w 6.0–6.5 (see Figure 2). This reflects the relative scarcity of large earthquakes ($M_w \geq 7.5$) in continental settings and the relative difficulty of studying small earthquakes ($M_w \leq 5$) using InSAR due to atmospheric noise, data incoherence or unfavorable earthquake depths. An additional factor limiting the number of small magnitude earthquakes used in this study is the absence of reported GCMT parameters for some of the small earthquakes studied using InSAR (e.g., for the M_w 5.0, 18 September 1997 and 1 October 1998 Zagros mountains earthquakes studied by *Lohman and Simons* [2005] and for the M_w 4.4, 21–22 September 2005, Kalannie and M_w 4.7, 10 October 2007, Katanning, Australia, earthquakes studied by *Dawson et al.* [2008]). Of the 57 earthquakes listed, 22 are strike-slip earthquakes, 13 have normal and 22 have thrust fault mechanisms. The InSAR data used to study these earthquakes are mainly C band data (for 51 earthquakes), with 9 events being studied using L band data, which were available for a relatively short time during this period. *Massonnet et al.* [1996], *Pritchard et al.* [2007] and *Pritchard and Fielding* [2008] used both C band and L band data to study the 1994 Northridge, California; the 1996 Nazca ridge, Peru; and the 2007 Pisco, Peru, earthquakes, respectively.

[10] In many of the published studies, InSAR data are combined with other types of data, such as GPS or seismic data. Thus, we split the database into different categories reflecting the data type used: I (InSAR data only; 61 source models in Tables 1–3), GI (GPS and InSAR data; 22 models in Tables 1–3), SI (seismic and InSAR data; 15 models in Tables 1–3) and OI (other and InSAR data, where other sources of information such as leveling, SPOT 5, and/or multiple combinations of data are used; 14 models in Tables 1–3). Whenever there are multiple studies of the same earthquake we include them in the database as they are valuable to assess uncertainties. Thus, for the 57 earthquakes studied, we obtain a total of 112 models in Tables 1–3.

[11] For a given published study we use solution(s), in order of importance, which are stated by the authors as their favorite solution and/or that fit the data better than other

Table 1. CMT Parameters From Published InSAR Studies for Earthquakes That Occurred Between 1995 and 1997[a]

Date	Location	M_0 (×10¹⁸ N m)	Lat (deg)	Long (deg)	Depth (km)	Strike (deg)	Dip (deg)	Rake (deg)	Type	Data	Reference
28.06.92	Landers	103.00	34.45	243.48	5.53	154.1	89.9	173.9	ss	GI	Fialko [2004]
29.06.92	*Little Skull Mountain*	*0.50*	*36.75*	*243.76*	*11.20*	*52.0*	*40.0*	*−51.0*	*n*	*I*	*Lohman et al. [2002]*
29.06.92	Little Skull Mountain	0.32	36.75	243.72	9.40	36.0	58.0	−78.0	n	SI	Lohman et al. [2002]
04.12.92	Fawnskin	0.15	34.35 ± 0.004	243.09 ± 0.002	2.60 ± 0.3	106.0 ± 7.0	28.0 ± 4.0	93.0 ± 4.0	th	I	Feigl et al. [1995]
04.12.92	Fawnskin	0.11	34.36 ± 0.001	243.09 ± 0.009	2.70 ± 0.15	102.0 ± 7.0	39.0 ± 4.0	92.0	th	I	Feigl and Thurber [2009]
20.03.93	Ngamr. County, Tibet	1.48 ± 0.02	29.06 ± 0.002	87.48 ± 0.003	7.00 ± 0.1	4.3 ± 1.0	49.7 ± 3.2	−99.4 ± 3.0	n	I	Funning [2005]
20.03.93	Ngamr. County, Tibet	1.57 ± 0.02	26.06 ± 0.002	87.49 ± 0.003	7.00 ± 0.1	4.2 ± 1.0	46.5 ± 2.8	−95.8 ± 2.5	n	SI	Funning [2005]
17.05.93	Eureka Valley, California	1.70 ± 0.3	37.11 ± 0.004	242.21 ± 0.005	9.20 ± 0.2	173.0 ± 2.0	54.0 ± 2.0		n	I	Massonnet and Feigl [1995]
17.05.93	Eureka Valley, California (DS)				13.00	7.0	50.0		n	I	Peltzer and Rosen [1995]
11.07.93	*N. Chile*	*18.00*	*−25.20*	*289.97*	*54.00*	*5.0*	*30.0*	*104.0*	*th*	*SI*	*Pritchard et al. [2006]*
29.09.93	Killari, India	1.76			3.25	95.0 ± 5.0	54.4	86.0 ± 5.0	th	I	Satyabala [2006]
17.01.94	Northridge	9.42				**248.0**	**42.0**		th	I	Massonnet et al. [1996]
26.05.94	Al Hoceima, Morocco	2.10	35.20	355.94	**7.00**	23.3 ± 4.5	86.9 ± 2.3	−1.2 ± 2.6	ss	I	Biggs et al. [2006]
26.05.94	Al Hoceima, Morocco (DS)	2.00				23.0	77.0		ss	I	Akoglu et al. [2006]
12.09.94	Nevada	0.92	38.82	240.38	7.84	319.0	72.0	152.0	ss/n	I	Amelung and Bell [2003]
16.01.95	Kobe, Japan	19.30	34.62	135.06	**6.22**	**229.1**	**89.9**	−114.4	ss	I	Ozawa et al. [1997]
13.05.95	Kozani-Grevena	6.50				254.0	48.0	−96.0	n	SI	Resor et al. [2005]
13.05.95	Kozani-Grevena	6.90 ± 0.5				257.8	38.2	−97.1	n	I	Rigo et al. [2004]
13.05.95	Kozani-Grevena	6.40							n	I	Meyer et al. [1996]
27.05.95	N. Sakhalin, Russia	73.73	52.89	142.90	7.29	197.5	84.2	173.7	ss	I	Tobita et al. [1998]
15.06.95	Aigion, Greece	3.90	38.33	22.22	5.10	275.0	35.0	−83.0	n	GI	Bernard et al. [1997]
30.07.95	Antofagasta, Chile (DS)	1600.00	−24.16	289.14	30.00	**5.0**	21.5	113.0	th	GI	Pritchard et al. [2002]
30.07.95	*Antofagasta, Chile*	*1800.00*	*−24.16*	*289.31*	*27.00*	***5.0***	*30.0*	*105.0*	*th*	*OI*	*Pritchard et al. [2006]*
01.10.95	Dinar, Turkey	4.55 ± 1.1	38.10	30.08	6.42 ± 3.1	145.0 ± 1.5	49.0 ± 1.0	**−90.0**	n	I	Wright et al. [1999]
01.10.95	Dinar, Turkey	4.30 ± 0.2	38.10 ± 0.009	30.09 ± 0.009	4.60 ± 0.1	135.0 ± 0.5	49.8 ± 0.9	−84.4 ± 3.6	n	I	Funning [2005]
01.10.95	Dinar, Turkey	3.70 ± 0.1	38.11 ± 0.009	30.09 ± 0.009	4.20 ± 0.1	135.2 ± 0.9	48.4 ± 0.9	−95.7 ± 2.3	n	SI	Funning [2005]
01.10.95	Dinar, Turkey (DS)	4.10				145.0	34.0		n	I	Fukahata and Wright [2008]
22.11.95	Nuweiba, Egypt	56.23	28.94	34.73	12.0	195.2	65.0	−15.5	ss/n	SI	Klinger et al. [2000]
22.11.95	Nuweiba, Egypt	70.00				200.0	80.0		ss	SI	Shamir et al. [2003]
22.11.95	Nuweiba, Egypt (DS)	65.00	28.88	34.75	11.25	197.5	67.0	−4.0	ss	SI	Baer et al. [2008]
19.04.96	*N. Chile*	*14.00*	*−23.94*	*289.94*	*49.00*	*5.0*	*23.0*	*107.0*	*th*	*SI*	*Pritchard et al. [2006]*
12.11.96	Nazca Ridge, Peru (DS)	440.00	−15.32	284.84	28.00	**307.0**	**30.0**	44.5	th	SI	Salichon et al. [2003]
12.11.96	*Nazca Ridge, Peru (DS)*	*480.00*	*−15.40*	*284.80*	*30.00*	*312.0*	*15.0–30.0*	*50.0*	*th*	*OI*	*Pritchard et al. [2007]*
26.03.97	Kagoshima, Japan	1.78				275.0 ± 6.0	81.0 ± 3.0	−19.0 ± 2.0	ss	GI	Fujiwara et al. [1998]
05.05.97	Zagros Mts, Iran (PS)	0.16	27.13 ± 0.003	53.88 ± 0.003	5.20 ± 3.0	120.0	80.0 ± 4.0	−90.0 ± 6.0	n	I	Lohman and Simons [2005]
05.05.97	Zagros Mts, Iran (FFP)	0.16	27.13 ± 0.003	53.88 ± 0.003	4.40 ± 3.0	120.0	80.0 ± 4.0	−90.0 ± 5.0	n	I	Lohman and Simons [2005]
05.05.97	Zagros Mts, Iran (DS)	0.16	27.12	53.89	6.20	**120.0**	**80.0**	−83.0	n	I	Lohman and Simons [2005]
26.09.97	Colfiorito, Italy 09h40 (DS)	0.48			4.50	**154.0**	**46.0**	**−77.0**	n	I	Salvi et al. [2000]
26.09.97	Colfiorito, Italy 00h33	0.98				**.0**	**45.0**	**−75.0**	n	SI	Salvi et al. [2000]
26.09.97	Colfiorito, Italy 00h33 (DS)	0.43				144.0	45.0	**−90.0**	n	GI	Stramondo et al. [1999]
26.09.97	Colfiorito, Italy 09h40 (DS)	1.05				144.0	45.0	**−90.0**	n	GI	Stramondo et al. [1999]
08.11.97	Manyi, Tibet	263.00	35.22	87.15	**6.38**	258.6	**89.8**	**−5.4**	ss	I	Funning et al. [2007]
08.11.97	Manyi, Tibet	171.90	35.26	87.21	4.85	**257.7**	89.1	−1.1	ss	I	Wang et al. [2007]
08.11.97	Manyi, Tibet (DS)	191.00	35.24	87.30	5.11	255.9	93.2	−5.7	ss	I	Wang et al. [2007]

[a]Date (day. month. year (dd. mm. yy)) and Location contain the earthquake's date and geographical location. M_0 is the seismic moment; Lat, Long, and Depth are the centroid's latitude, longitude, and depth, respectively; Strike, Dip, and Rake are the fault's strike, dip, and rake angles, respectively. Type is the type of faulting indicated by ss (strike-slip fault), n (normal fault), and th (thrust fault). Data is the type of data used for a given study: I (using InSAR data only), SI (using seismic and InSAR data), and OI (using InSAR data combined with two or more other types of data; see text for details). Whenever there are multiple models of the same earthquake produced in a given study, we distinguish them using the following: DS (distributed slip model), PS (point source model), FFP (finite fault patches), 1 seg. (fault model only with one segment), mult. seg. (fault model with multiple segments), PM (planar model) and CM (curved model). Models in italic correspond to InSAR solutions obtained using layered elastic media in the deformation modeling. Parameters in bold were fixed in the InSAR inversions. Blank spaces mean that we were not able to obtain the corresponding source parameters.

Table 2. Same as Table 1 but for Earthquakes Occurring Between 1998 and 2003

Date	Location	M_0 ($\times 10^{18}$ N m)	Lat (deg)	Long (deg)	Depth (km)	Strike (deg)	Dip (deg)	Rake (deg)	Type	Data	Reference
10.01.98	Zhangbei, China	0.48	41.14 ± 0.004	114.44 ± 0.004	5.40 ± 0.3	200.8 ± 6.4	42.7 ± 3.6	85.9 ± 10.2	th	I	Li et al. [2008]
10.01.98	Zhangbei, China (DS)	0.47	41.13	114.51	5.00	200.8	42.7	85.9	th	I	Li et al. [2008]
30.01.98	N. Chile	61.00	−23.96	289.83	45.00	5.0	23.0	102.0	th	SI	Pritchard et al. [2006]
14.03.98	Fandoqa, Iran	8.90 ± 1.4	30.03 ± 0.004	57.64 ± 0.004	3.50 ± 0.3	145.2 ± 1.1	63.2 ± 2.2	−151.6 ± 11.5	ss	I	Funning [2005]
14.03.98	Fandoqa, Iran	8.28	30.01	57.64	3.67	150.0	52.0	−146.0	ss	I	Berberian et al. [2001]
14.03.98	Fandoqa, Iran	8.40 ± 0.4	30.02 ± 0.004	57.65 ± 0.002	3.50 ± 0.2	147.3 ± 1.1	65.1 ± 3.2	−154.1 ± 3.44	ss	SI	Funning [2005]
22.05.98	Aiquile, Bolivia (DS)	8.44	−17.89	294.82	7.30	7.0	79.0	171.0	ss	I	Funning et al. [2005b]
22.05.98	Aiquile, Bolivia	7.77	−17.90	294.84	7.40	7.0	79.0	171.0	ss	I	Funning et al. [2005b]
03.09.98	Mt Iwate, Japan (DS)	1.40	39.80	140.90	1.30	200.0	35.8	112.0	th	GI	Nishimura et al. [2001]
28.03.99	Chamoli, Himalaya	2.70	30.44	79.39		300.0	15.0	90.0	th	I	Satyabala and Bilham [2006]
30.04.99	Zagros Mts, Iran (PS)	0.112	27.87 ± 0.002	53.63 ± 0.002	4.10 ± 0.18	110.0	42.0 ± 6.0	−85.0 ± 7.0	n	I	Lohman and Simons [2005]
30.04.99	Zagros Mts, Iran (FFP)	0.112	27.87 ± 0.002	53.63 ± 0.002	3.20 ± 0.15	110.0	53.0 ± 5.0	−77.0 ± 13.0	n	I	Lohman and Simons [2005]
30.04.99	Zagros Mts, Iran (DS)	0.112	27.87	53.63	5.30	110.0	53.0	−79.0	n	I	Lohman and Simons [2005]
17.08.99	Izmit, Turkey	253.59	40.73	30.05	10.80	271.2	89.7	−173.1	ss	I	Wright [2000]
17.08.99	Izmit, Turkey (DS)	184.00					85.0		ss	OI	Feigl et al. [2002]
17.08.99	Izmit, Turkey (DS)	240.00	40.72	30.21	7.90	267.6	85.0	179.6	ss	OI	Delouis et al. [2000]
17.08.99	Izmit, Turkey (DS)	190.00	40.72	30.07	6.99	90.7	88.3	178.7	ss	OI	Cakir et al. [2003]
07.09.99	Athens, Greece Model 1	1.29	38.09	23.63	9.50	100.0	43.0		n	I	Kontoes et al. [2000]
07.09.99	Athens, Greece Model 2	1.46	38.11	23.63	9.50	116.0	54.0		n	I	Kontoes et al. [2000]
16.10.99	Hector Mine (DS)	72.00	34.56	243.73	1.90	153.3	85.3	177.4	ss	GI	Simons et al. [2002]
16.10.99	Hector Mine (DS)	59.30	34.56	243.73	6.08	332.3	83.0	184.6	ss	GI	Jonsson et al. [2002]
16.10.99	Hector Mine (DS)	58.00	34.58	243.72	4.89	332.7	81.4	176.0	ss/th	OI	Salichon et al. [2004]
12.11.99	Duzce, Turkey 1 seg.	65.60 ± 3.4	40.80	31.27	6.30 ± 1.0	259.0 ± 1.0	51.0 ± 4.0	−178.0 ± 3.0	ss	I	Wright [2000]
12.11.99	Duzce, Turkey Mult. seg.	41.46	40.81	31.21	7.65	273.9	57.0 ± 4.0	−134.0 ± 17.0	ss	I	Wright [2000]
12.11.99	Duzce, Turkey	51.40	40.72	31.26	6.77	84.5	56.7	−174.0	ss/n	GI	Burgmann et al. [2002]
12.11.99	Duzce, Turkey (DS)	56.60				86.7	54.0		ss/n	GI	Burgmann et al. [2002]
06.06.00	Cankiri, Turkey	1.40	40.63	32.99	5.50	357.0 ± 15.0	55.0 ± 19.0	−20.0 ± 15.0	n	I	Cakir and Akoglu [2008]
06.06.00	Cankiri, Turkey	1.38	40.63	32.99	4.0–6.6	2.0	33.0	−37.0	n	I	Pedersen et al. [2001]
17.06.00	S. Iceland	5.42	63.96	339.65	4.99	5.0	86.0	175.0	ss	GI	Pedersen et al. [2003]
17.06.00	S. Iceland	4.40	63.97	339.66	3.94	1.0	87.0	180.0	ss	GI	Pedersen et al. [2003]
17.06.00	S. Iceland (DS)	4.50	63.97	339.66	3.09	2.0	87.0	180.0	ss	GI	Pedersen et al. [2001]
21.06.00	S. Iceland	5.06	63.99	339.30	4.50	359.0	90.0	180.0	ss	I	Pedersen et al. [2003]
21.06.00	S. Iceland	5.30	63.99	339.30	4.10	0.0	90.0	180.0	ss	GI	Pedersen et al. [2003]
21.06.00	S. Iceland (DS)	5.00	63.98	339.30	2.97	0.0	90.0	180.0	ss	GI	Schmidt and Burgmann [2006]
26.01.01	Bhuj, India	190.00	23.51	70.27	13.00 ± 1.1	82.0	51.0	77.0	th	I	Schmidt and Burgmann [2006]
26.01.01	Bhuj, India (DS)	250.00				82.0	51.0		th	I	Bustin et al. [2004]
28.02.01	Nisqually	20.00	47.10	237.33	51.00	180.0	20.0		n	GI	Bustin et al. [2004]
28.02.01	Nisqually				60.0	180.0	20.0		n	GI	Pritchard et al. [2007]
23.06.01	Arequipa, Peru (DS)	6300.00	−17.36	287.39	27.00	316.0	11–25	69.0	th	OI	Lasserre et al. [2005]
14.11.01	Kokoxili, Tibet (DS)	710.00	35.84	92.45	11.00	97.6	90.0	0.0	ss	I	Wright et al. [2003]
23.10.02	Nenana Mountain Alaska	10.80 ± 0.8	63.50 ± 0.002	211.95 ± 0.004	12.90 ± 0.7	261.8 ± 0.9	81.2 ± 1.7	173.7 ± 1.3	ss	I	Wright et al. [2004a]
03.11.02	Denali, Alaska	649.82	63.22	214.85	6.93	108.5	84.4	171.9	ss	GI	Belabbès et al. [2009]
21.05.03	Zemmouri, Algeria (PM)	17.80	35.84			65.0	40.0	90.0	th	OI	Belabbès et al. [2009]
21.05.03	Zemmouri, Algeria (CM)	21.50				65.0	40.0	90.0	th	OI	Nishimura et al. [2003]
26.07.03	Miyagi, Japan	1.80	38.45	141.19	2.29	212.2	38.7	102.7	th	OI	Funning et al. [2005a]
26.12.03	Bam, Iran	9.00 ± 0.3	29.03	58.36	5.69	355.4	89.9	−173.5	ss/th	I	Funning et al. [2005a]
26.12.03	Bam, Iran	6.20 ± 0.4	29.04	58.36	4.70 ± 0.4	355.2 ± 1.0	86.6 ± 3.6	173.7 ± 1.7	ss/th	SI	Peyret et al. [2007]
26.12.03	Bam, Iran	5.00	29.05	58.35	5.8	359.6	86.0	−179.8	ss	I	Peyret et al. [2007]
26.12.03	Bam, Iran		29.06	58.36	4.8	1.6	88.0	−170.9	ss	OI	Motagh et al. [2006]
26.12.03	Bam, Iran (DS)	6.79			5.60	358.2	88.8	180.0	ss	OI	

Table 3. Same as Table 1 but for Earthquakes Occurring Between 2004 and 2007

Date	Location	M_0 (×10^{18} N m)	Lat (deg)	Long (deg)	Depth (km)	Strike (deg)	Dip (deg)	Rake (deg)	Type	Data	Reference
24.02.04	Al Hoceima, Morocco	6.20	35.14	356.01	**10.05**	295.4 ± 1.1	87.4 ± 1.5	−179.2	ss	I	*Biggs et al.* [2006]
24.02.04	Al Hoceima, Morocco (DS)	7.40	35.14	356.00	8.80	**295.0**	**88.0**	**−179.0**	ss	I	*Biggs et al.* [2006]
24.02.04	Al Hoceima, Morocco	5.88	35.17	355.98	6.90	339.5	88.0	178.0	ss	OI	*Tahayt et al.* [2009]
24.02.04	Al Hoceima, Morocco (DS)	6.60							ss	I	*Akoglu et al.* [2006]
24.02.04	Al Hoceima, Morocco (DS)	6.80					88.0		ss	I	*Cakir et al.* [2006]
24.10.04	Niigata, Japan	13.99	37.30	138.83	4.70	200.0	45.0	72.0	th	I	*Ozawa et al.* [2005]
22.02.05	Zarand Iran	6.70 ±0.2	31.50	56.80	4.65 ±0.3	266.0 ±1.0	67.0 ±2.0	105.0 ±2.0	th	I	*Talebian et al.* [2006]
20.03.05	Fukuoka-ken Seiho-oki, Japan	7.10				298.0	79.0	−18.0	ss	GI	*Nishimura et al.* [2006]
20.03.05	Fukuoka-ken (DS) Seiho-oki, Japan	8.70							ss	GI	*Nishimura et al.* [2006]
13.06.05	Tarapaca, Chile	580.00				189.0	24.0	−74.0	n	OI	*Peyrat et al.* [2006]
08.10.05	Kashmir (DS)	336.00	34.29	73.77		**321.5**	**31.5**		th	I	*Pathier et al.* [2006]
27.11.05	Qeshm Island, Iran	1.27 ± 0.07	26.77	55.92	6.00	267.0 ± 2.0	49.0 ± 4.0	105.0 ± 5.0	th	I	*Nissen et al.* [2007]
31.03.06	Chalan-Chulan, Iran	1.70	33.67	48.88	4.80	**320.0**	60.0	**180.0**	ss	I	*Peyret et al.* [2008]
31.03.06	Chalan-Chulan, Iran (DS)	1.58				**320.0**	60.0	**180.0**	ss	I	*Peyret et al.* [2008]
25.03.07	Noto Hanto	14.52	37.22	136.66	6.00	**50.7**	53.5	150.0	th	GI	*Ozawa et al.* [2008]
25.03.07	Noto Hanto (DS)	11.09				**50.7**	48.0	115.0	th	GI	*Fukushima et al.* [2008]
15.08.07	Pisco, Peru	1900.00	−13.89	283.48	30.00	**316.0**	11–25	71.0	th	SI	*Pritchard and Fielding* [2008]

solutions. Whenever uniform and variable slip inversions are carried out, we include both final inversion solutions in the database, except if any of the models has a substantially lower misfit or if it is indicated by the authors as not being a preferred model. We use all the information provided in the papers (as well as provided on request by authors) to maximize our set of source parameters. Nevertheless, for many studies not all the required parameters are given (particularly the centroid location). For example, often the location of the fault's corner or the updip surface projection of the centroid
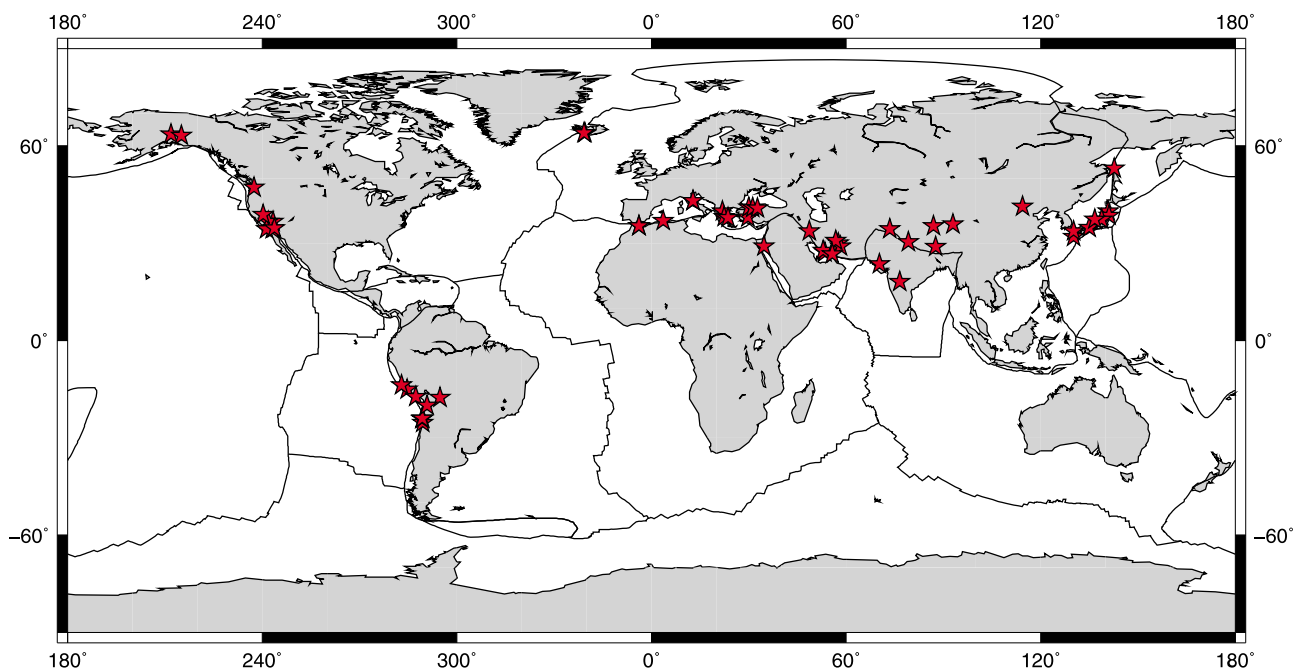
Figure 1. Geographical location of the 57 earthquakes (stars) studied with InSAR used in this study. All earthquakes have magnitudes between M_w 5.0 and 8.5 and are shallow (depth less than 60 km), except for the 2005 Tarapaca, Chile, earthquake (GCMT depth is 97.6 km).
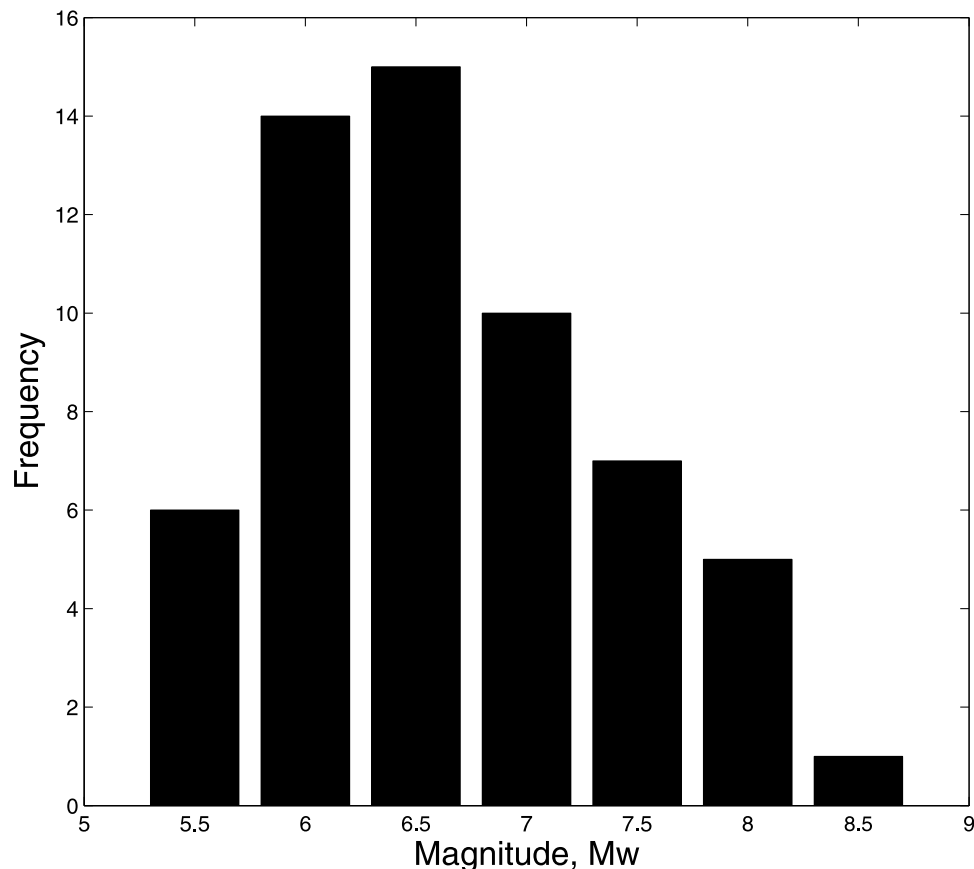
Figure 2. Distribution of earthquake moment magnitudes (M_w) of the earthquakes studied with InSAR used in this study. The distribution is skewed toward earthquakes in the magnitude range 6–6.5. This is probably due to the higher frequency of earthquakes of that magnitude compared to larger events and to a higher detectability of such earthquakes using InSAR than to smaller events. Also, in this study we do not use a number of small earthquakes studied using InSAR because of the absence of reported GCMT parameters for them (see text for details).

are given, rather than the actual centroid location. In these cases we compute the parameters from published and/or provided information; for uniform slip models, centroid locations are calculated using geometrical information (e.g., location of corner of fault, fault strike, dip, width and length). For the variable slip models that we obtained from several authors, we calculate centroid locations using the spatial distribution of slip combined with fault geometry. Also, often the seismic moment, M_0, is not given. We use

$$M_0 = \mu \, A \, \bar{u}, \qquad (1)$$

where M_0 is the seismic moment, μ is the rigidity modulus, A is the fault's area and $\bar{u}$ is the average slip. We use the rigidity modulus quoted in the study or in other studies of earthquakes in the same region (or by the same authors); failing that, we use a standard rigidity modulus of $\mu = 32$ GPa. Where faults are segmented, with changes in width along strike, the total moment is computed and a weighted average based on the seismic moment for each segment is used to determine overall parameters (centroid location and fault strike, dip and rake).

[12] In this study we do not use InSAR source models where multiple subevents are present that are clearly spatially discontinuous. We also discard from this study a few InSAR solutions that the authors state as being strongly influenced by substantial postseismic deformation, such as, for example, the 2004 Parkfield earthquake.

2.1. Example of Calculation of ICMT Parameters

[13] In this section we illustrate our approach by calculating ICMT parameters for the two-fault, uniform slip model for the 2003 Bam, Iran, earthquake produced by *Funning et al.* [2005a]. This model consists of two subfaults with individual focal mechanisms as shown in Figure 3. The primary fault released a seismic moment of 7.6×10^{18} N m, whereas the secondary fault has a seismic moment of 1.4×10^{18} N m. Figure 3 shows the focal mechanism (red beach ball) obtained from the total moment and the moment-weighted average strike, dip and rake of the two faults, assuming a pure double-couple source mechanism (see overall parameters in Table 2). As expected, the focal mechanism obtained from the overall parameters is similar to that of the primary fault, which has the larger moment. We also show the geometric centroid of each fault (black crosses) and the overall centroid obtained from a moment-weighted average of the centroids of the two faults (red
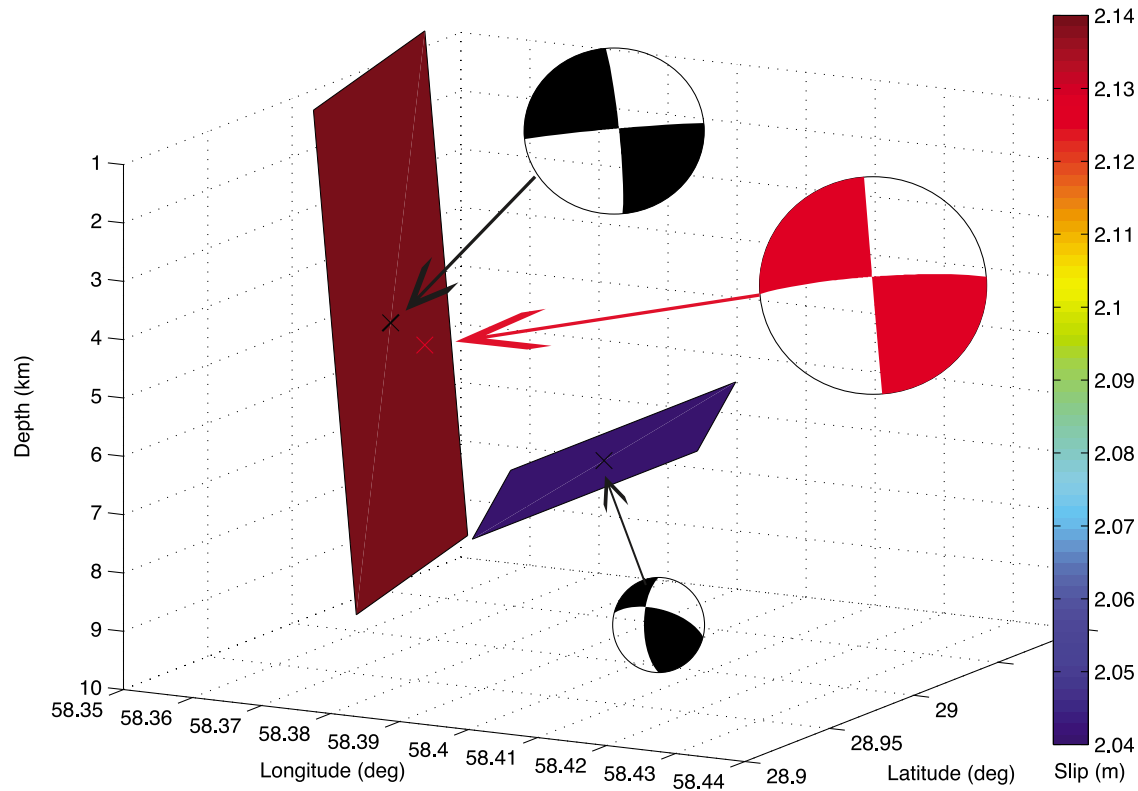
Figure 3. Example of calculation of overall CMT source parameters for the 2003 Bam earthquake, using the two-fault, uniform slip model of *Funning et al.* [2005a] obtained using InSAR data. The model consists of a main fault plane with 2.14 m of slip and a smaller secondary fault with 2.04 m of slip, with estimated seismic moments of 7.6×10^{18} and 1.4×10^{18} N m, respectively. The corresponding focal mechanisms (black beach balls) and centroid locations (black crosses) are shown. The red beach ball represents the focal mechanism obtained from the total moment and from the moment-weighted average of strike, dip and rake of the two faults, assuming a pure double-couple mechanism. The average centroid location is also shown (red cross). The beach balls are not in absolute scale.

cross). Again, as expected, the overall centroid is close to that of the primary fault.

3. Analysis of the Variability of InSAR Source Models for a Given Earthquake

[14] Since the earthquakes used in this study span 15 years and the InSAR source models are generally built using different data sets and modeling strategies, our compilation is nonuniform in terms of reliability of the various models. For some cases, the compilation contains several source models for a given earthquake. The variability in such earthquake source models provides a means to qualitatively assess the generally unknown uncertainties of the source parameters.

3.1. Seismic Moment

[15] Among the 29 earthquakes in our compilation with several InSAR-derived estimates of seismic moment, the intraevent variability in moment between the smallest reported value and the others is smaller than 20% for 19 earthquakes (with a median of about 17% and standard deviation of 11 percentage points, $\sigma = 11\%$). Larger variabilities occur for the following seven earthquakes: 2003 Bam (44% difference between the moment estimated by

Peyret et al. [2007] and that obtained by *Funning et al.* [2005a]; see Table 2); 1992 Little Skull Mountain (36% difference between "InSAR only" and "seismic and InSAR" models determined by *Lohman et al.* [2002], see Table 1); 1997 Manyi (35% difference between the moment by *Funning et al.* [2007] and that by *Wang et al.* [2007]; see Table 1); 1999 Duzce (37% difference between the moment obtained using a one-segment versus a multiple-segment model by *Wright* [2000]; see Table 2); 1992 Fawnskin (27% difference between the moment by *Feigl and Thurber* [2009] and that by *Feigl et al.* [1995]; see Table 1); and 1999 Izmit (25% difference between the moment by *Feigl et al.* [2002] and by *Wright* [2000]; see Table 2). The latter discrepancy may be in particular due to contamination by postseismic deformation, which was taken into account by *Feigl et al.* [2002].

3.2. Fault Geometry and Mechanism

[16] Differences in strike for a given earthquake are generally smaller than 20° (with a median variability over 18 earthquakes of about 4° and $\sigma = 10°$), except for the Al Hoceima 2004 earthquake, for which there is a difference of 44° between the strike determined by *Tahayt et al.* [2009] and that found by *Biggs et al.* [2006] (see Table 3). For the 19 earthquakes in Tables 1–3 with more than one value

of fault dip reported, the variability in dip is smaller than 20° (with a median of about 8° and $\sigma = 6°$), except for the 2000 Cankiri earthquake, for which there is a difference of 22° between the fault dip determined by *Wright* [2000] and that obtained by *Cakir and Akoglu* [2008]. The variability in rake for a given earthquake is also generally smaller than 20° (with a median over 21 earthquakes of about 7° and $\sigma = 11°$), except for the following earthquakes: 1992 Little Skull (27° difference; see Table 1), 1999 Duzce (44° difference; see Table 2) and 2007 Noto Hanto (35° difference; see Table 3).

3.3. Centroid Spatial Location

[17] Differences in epicentral location for a given earthquake are smaller than 10 km for 18 earthquakes (with a median over 20 earthquakes of about 3 km and $\sigma = 5$ km), with the following three earthquakes showing larger differences: 1995 Antofagasta (17 km difference between the studies of *Pritchard et al.* [2002, 2006]); 1997 Manyi (14 km difference between the results of *Funning et al.* [2007] and *Wang et al.* [2007]); and 1999 Izmit (14 km between the results of *Wright* [2000] and *Delouis et al.* [2000]). There is a very good agreement between the centroid depths in the various InSAR source models for a given earthquake, with a variability smaller than 5 km for most earthquakes (with the median of the variabilities for 20 earthquakes being about 2 km and $\sigma = 2$ km). The maximum variability in depth is of 9 km for the 2001 Nisqually earthquake between source models obtained using layered 1-D and 3-D media by *Bustin et al.* [2004].

4. Comparisons Between Seismically and Geodetically Derived Earthquake Source Parameters

[18] In this section we compare the various ICMT parameters with those in three different seismic catalogs: the Global CMT (GCMT) catalog, the ISC catalog and the EHB catalog. In order to reduce the effect of the nonhomogeneity of our ICMT compilation on the comparisons, we do not use a few InSAR solutions for which the authors clearly state that there is low signal-to-noise ratio in the InSAR data or potential contamination of the signal by aftershocks or by postseismic deformation.

4.1. Seismic Moment

[19] Figure 4 compares seismic moment values from the Global CMT catalog with estimates from 96 InSAR source models. Overall, the differences in seismic moment calculated using these two techniques are relatively small, following a distribution close to Gaussian with a median of −3.2%, an average of 4.1% and a standard deviation of 34.1%. We find that the mean difference between InSAR and GCMT moment values is not statistically significantly different from zero at a 95% confidence interval (Student's *t* test). This disagrees with previous studies using fewer earthquakes [e.g., *Feigl et al.*, 2002; *Lohman and Simons*, 2005] and using simulations [*Dawson et al.*, 2008], which suggested that seismic moments determined using InSAR were larger than those obtained from seismic data. If anything, we find a slight tendency of InSAR predicting smaller seismic moments than those reported in the Global CMT catalog.

[20] There is no relationship between differences in seismic moment and the specific combination of data used to determine the InSAR solutions: I, GI, SI, OI (see Figure 4b); likewise, there is no dependence of the differences of seismic moment on the size of the earthquake. We also examine the differences in seismic moment as a function of postseismic time elapsed between the earthquake and the latest InSAR data used to investigate potential effects of contamination by postseismic deformation, but do not find any clear relationship (see Figure S2a in the auxiliary material).[1] Moreover, we examine the differences in seismic moment as a function of the non-double-couple component of the earthquakes in the Global CMT catalog to investigate whether the discrepancies were larger for earthquakes with reported large non-double-couple component but do not find any clear dependency (see Figure S2b). In addition, we examine the differences in seismic moment as a function of strike, dip, rake and earthquake depth and do not find any clear trend (see Figure S2, which shows all these comparisons). Analyzing the differences in seismic moment as a function of fault mechanism, it seems that for thrust earthquakes there is a slight tendency for InSAR to overestimate the seismic moment compared to GCMT moment values (see captions of Figure S2). However, our moment comparisons only include 24 thrust earthquake models and the standard deviation of the differences is large, so this tendency is not statistically significant. We also split the set of seismic moments into two subsets corresponding to InSAR determinations using uniform and variable slip models; we found similar tendencies in the comparisons between InSAR and GCMT moments for these two subsets to that found in Figure 4 (see Figure S3). Among all the InSAR models used here, only fifteen report uncertainties for the estimated seismic moments (see Tables 1–3); the observed trend in the differences in seismic moment between InSAR and GCMT does not change when taking these uncertainties into account. We also compare moment magnitudes M_w calculated from the InSAR and GCMT seismic moments; Figure S2 shows that the differences in M_w are small (generally smaller than 0.16) and broadly normally distributed with a median of −0.0093.

[21] For some studies there are large differences between seismically and InSAR-determined moments. For example, for the 1994 Al Hoceima earthquake there are differences in moment of over 100% between the InSAR solutions of *Biggs et al.* [2006] and *Akoglu et al.* [2006] and the Global CMT solution, corresponding to a difference in M_w of 0.2, with the InSAR moment being larger than that in the GCMT catalog. A possible reason for this is that a substantial amount of surface deformation for this earthquake was offshore and the onshore deformation was relatively small, thus the signal-to-noise ratio in the interferogram was relatively low, which makes InSAR determinations more difficult. As a result, *Biggs et al.* [2006] report a strong trade-off between slip and length, which might have affected moment estimations. Likewise, for the 1993 northern Chile earthquake the InSAR moment estimated by *Pritchard et al.* [2006] is 78% larger than that reported in the GCMT catalog, leading to a moment magnitude difference of 0.17.
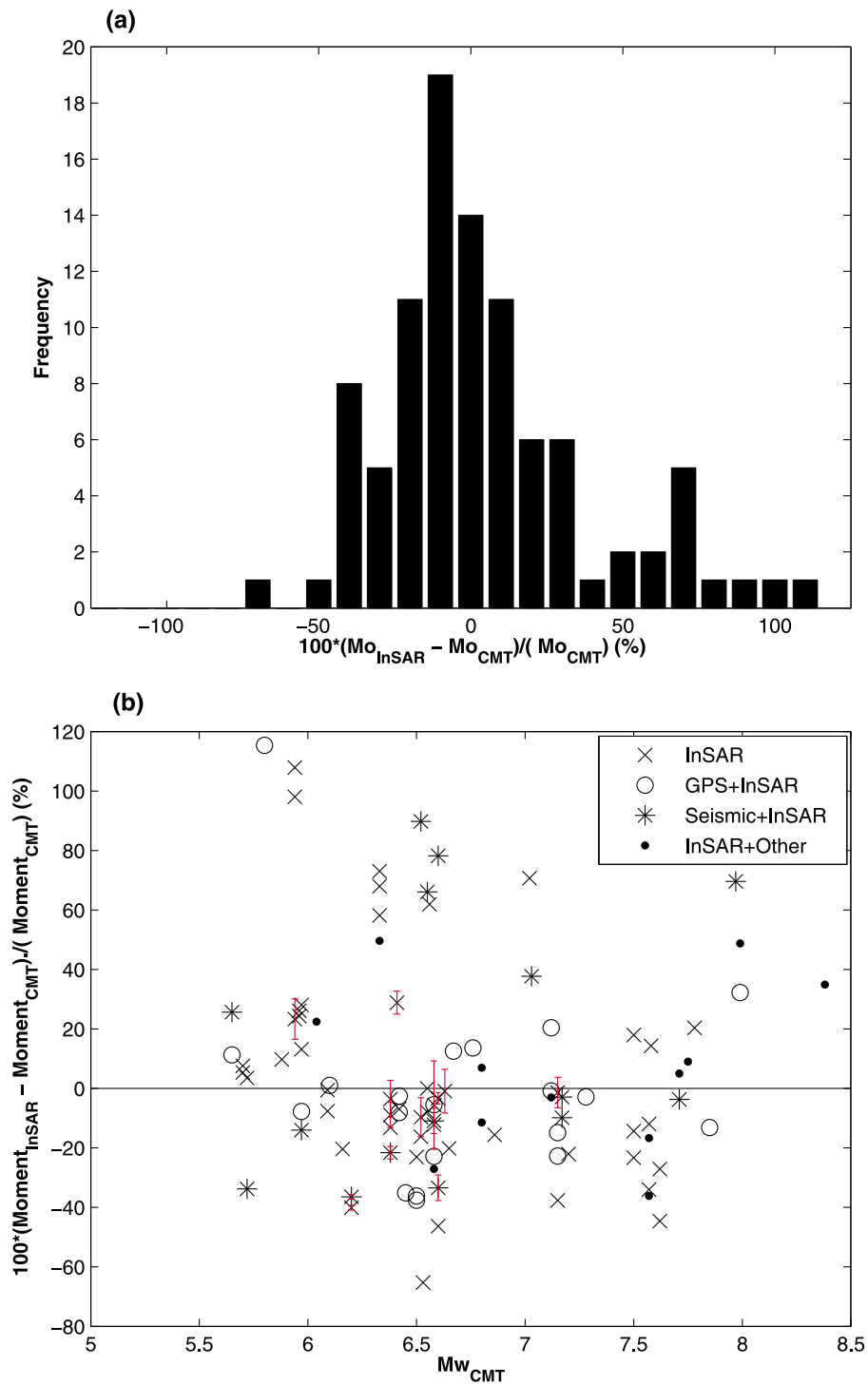
Figure 4. (a) Distribution of the percentage difference in seismic moment between InSAR and Global CMT determinations, for earthquakes investigated using InSAR in 96 studies published in the literature. (b) Percentage difference between InSAR and Global CMT seismic moment as a function of InSAR moment. Median is −3.2%; $\sigma = 34.1\%$. The errors in seismic moment estimated in some InSAR studies are taken into account and are shown in red.

Possible reasons for this discrepancy are that Pritchard et al. use a single interferogram, lacking offshore data coverage, and the signal-to-noise ratio is low for this relatively small and deep earthquake. For the 1999 Chamoli, Himalaya earthquake, the InSAR moment estimated by *Satyabala and Bilham* [2006] is about 65% smaller than that in the GCMT, leading to a magnitude difference of −0.3 between the InSAR and GCMT estimates. This may be due to the fact that this earthquake occurred in a mountainous region, which does not present ideal conditions for InSAR mea-

(a)

(b)

(c)
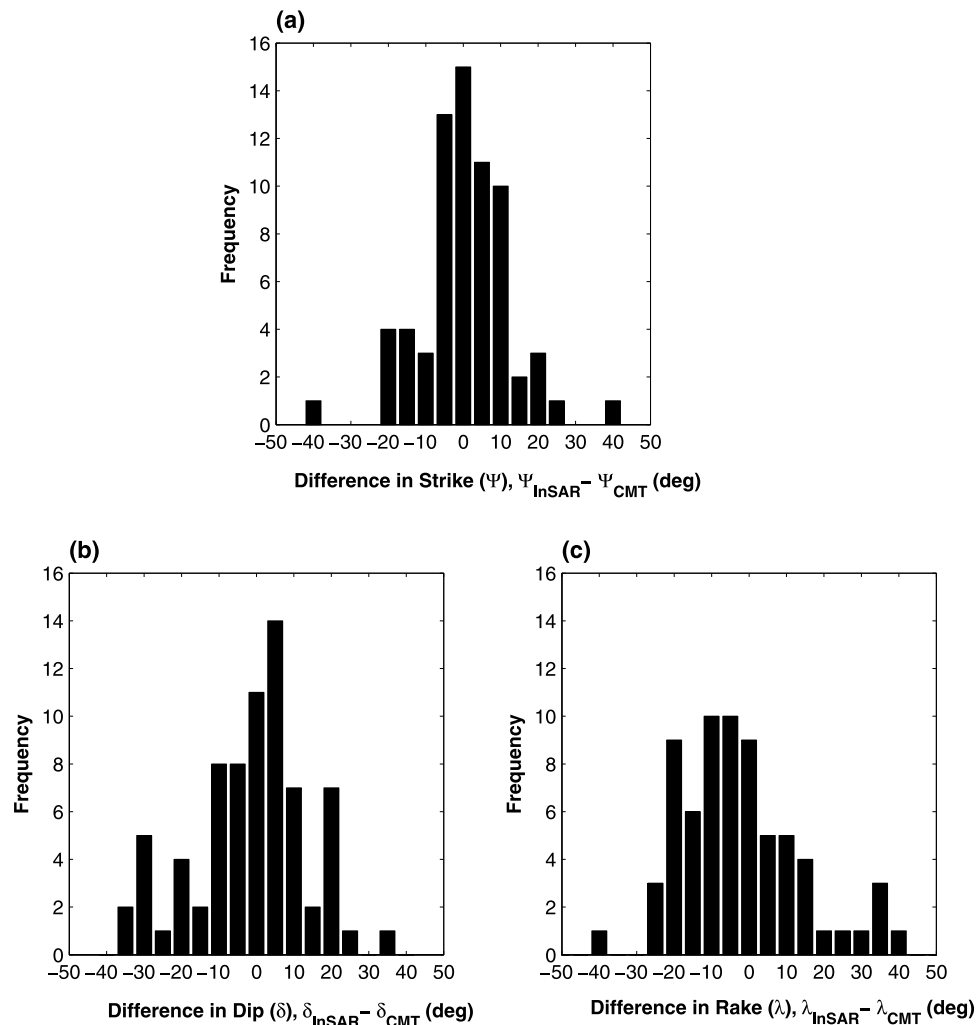
Figure 5. (a) Distribution of the difference in earthquake fault strike between InSAR and Global CMT determinations using 68 InSAR strike values published in the literature. The median and standard deviation of the distribution are 1.0° and 12.0°, respectively. (b) Distribution of the difference in fault dip between InSAR and Global CMT determinations using 73 InSAR dip values published in the literature. The median and standard deviation of the distribution are 1.0° and 15.1°, respectively. (c) Distribution of the difference in fault rake between InSAR and Global CMT determinations using 69 InSAR rake values published in the literature. The median and standard deviation of the distribution are −6.0° and 16.4°, respectively.

surements; a 50° slope was facing the radar for both ascending and descending tracks [*Satyabala and Bilham*, 2006]. Thus, InSAR may have not been able to detect all the surface deformation caused by the event and hence led to an underestimation of the seismic moment. In addition, for the 2003 Bam earthquake, all InSAR studies [*Funning et al.*, 2005a; *Motagh et al.*, 2006; *Peyret et al.*, 2007] estimated a smaller magnitude than that reported by the GCMT catalog, with the estimate by *Peyret et al.* [2007] having the largest discrepancy, with a moment of 46% smaller than the GCMT, which corresponds to a difference in moment magnitude of about −0.18. A potential source of error when estimating the horizontal motion close to the rupture is the angle at which the satellite acquired the data, combined with the fault's orientation. Other possible causes are the paucity of well-correlated pixels on the west side of the fault in some studies and the use of different smoothing parameters

in the source inversions. This is further supported by the large intraevent variability in seismic moment obtained using InSAR for this earthquake, as discussed in section 3.1. Finally, for the 2001 Bhuj earthquake, the seismic moment determined by *Schmidt and Burgmann* [2006] is 45% smaller than that reported by the GCMT catalog, corresponding to a moment magnitude difference of about −0.17. Poor InSAR data for this earthquake is a possible reason for this discrepancy, as the earthquake's region is characterized by low lying vegetated land, which was flooded at the time of the earthquake. Consequently, there is a lack of coherence in the epicentral region and the near surface slip is not well constrained.

4.2. Fault Geometry and Mechanism

[22] Figure 5 compares fault strike, dip and rake estimated using InSAR with the values reported in the Global CMT

catalog. We do not consider strike, dip and rake values that were held fixed in some InSAR studies (see Tables 1–3). Overall, there is a good agreement between fault strike, dip and rake determined by these two techniques, with differences following a distribution close to normal, centered around zero. The distribution of differences in strike has the smallest standard deviation, with most strike differences being smaller than 20°. The greatest difference in strike is 44°, for the model by *Tahayt et al.* [2009] of the 2004 Al Hoceima earthquake, which was also found to be quite different to other InSAR strike estimations, as discussed in section 3.2. A possible explanation for this discrepancy is that this model is a cross fault model, consisting of two subevents separated by about 3 s [e.g., *Stich et al.*, 2005] being quite different from a point source model, such as used in the GCMT approach. The distribution of differences in dip is also centered around zero, with most fault dip angle differences being smaller than 20°, but shows a greater spread. The distribution of differences in rake shows the greatest spread, with a maximum difference in rake of 42° for the earthquake model by *Ozawa et al.* [2008] for the 2007 Noto Hanto earthquake. A possible reason for this discrepancy is that this earthquake occurred on the coast of the Noto peninsula, thus limiting the use of InSAR data. Moreover, this difference may also be due to limitations in the GCMT technique, as the rake value determined by *Ozawa et al.* [2008] is more compatible with that determined using regional seismic data [*Ozawa et al.*, 2008].

[23] We do not find any relationship between differences in strike, dip and rake and the type of data used in the InSAR modeling (InSAR only, InSAR and GPS, InSAR and seismic, InSAR and other). Moreover, we examined the differences in strike, dip and rake as a function of other parameters such as seismic moment, postseismic elapsed time, non-double-couple component of the earthquakes reported in the Global CMT catalog and earthquake depth, and did not find any clear relationship (see Figures S4–S6, which show all these comparisons).

4.3. Centroid Spatial Location

4.3.1. Epicentral Location

[24] Figure 6 shows the distribution of epicentral distance between InSAR-determined and seismically determined epicenters from the GCMT, ISC and EHB catalogs, and Figure 7 shows the corresponding mislocation arrows. The differences in centroid epicenter are greater for the GCMT catalog (Figure 6), which shows a distribution of differences with a median of about 21 km and a standard deviation of $\sigma \approx 13$ km. A number of solutions show epicentral distances between InSAR and the GCMT larger than 40 km, particularly for subduction earthquakes in South America: 2007 Pisco [*Pritchard and Fielding*, 2008]; 1993, 1996 and 1998 northern Chile [*Pritchard et al.*, 2006] and 1996 Nazca Ridge [*Salichon et al.*, 2003]. This is probably due to the fact that seismic locations tend to be systematically mislocated in these subduction zones toward the trench [e.g., *Syracuse and Abers*, 2009]. However, the InSAR locations might also be systematically located landward due to a lack of InSAR data coverage offshore. For the 1992 Little Skull Mountain earthquake, there is an epicentral difference of about 42 km between the GCMT location and that by *Lohman et al.* [2002]. This is possibly due to limitations in

the GCMT method, as there is a disagreement in location of up to 11 km between different seismic studies [*Lohman et al.*, 2002].

[25] Epicentral differences are smaller for the ISC and EHB catalogs, which show narrower distributions with medians of about 9 km and 11 km, respectively. For these catalogs all differences in epicentral location are generally smaller than 40 km, except for the 1998 Aiquile earthquake. There is a difference of about 40 km between the ISC epicentral location and the InSAR location obtained by *Funning et al.* [2005b] using an uniform slip model, which is consistent with the damage distribution for that event. It is important to note though that the epicentral distance comparisons for the ISC and EHB catalogs contain 7 fewer comparisons than for the GCMT. The reason for this is that we do not carry out comparisons for very large earthquakes ($M_w \geq 7.7$) because for such large earthquakes the earthquake centroid (as determined by InSAR) will be different to the rupture's initiation point (reported by ISC and EHB) and thus the comparisons would be inappropriate.

[26] In some cases, the seismic epicentral mislocation arrows relative to the InSAR solutions show some geographic consistency, such as in South America (Figure 7) and in Morocco, Greece and Turkey (Figure 8). However, for other regions, there is no geographic consistency, such as in Iran and in California (Figure 8).

[27] We do not find any relationship between the seismic-InSAR epicentral differences and any other parameters such as seismic moment, earthquake depth, type of earthquake mechanism, type of data used in the InSAR modeling, non-double-couple component of the earthquake and postseismic time elapsed (see Figure S7, which shows all these comparisons).

4.3.2. Depth

[28] Figure 9 ($M = 0.150$) shows differences between InSAR centroid depth estimates and depth values reported in the EHB catalog obtained from free depth determinations. We do not carry out comparisons for depth values reported in the GCMT catalog because for most earthquakes in this study the depths in the catalog are fixed at 15 km. Moreover, we do not show comparisons with ISC depths, because the results are very similar to those obtained using depths in the EHB catalog. With the exception of a few outliers, Figure 9 shows that differences between InSAR and EHB depths are relatively small, with a median difference on the order of 5 km. The largest difference in depth occurs for the 2005 Qeshm earthquake, where the InSAR depth determined by *Nissen et al.* [2007] is 39 km shallower than that reported by EHB. The same authors also use teleseismic data to determine a depth that is 36 km shallower than that reported by the EHB catalog; thus, this difference probably results from limitations in the EHB method. The distribution of depth differences is biased toward InSAR depths being shallower than EHB depths, which is consistent with previous studies (see, e.g., *Feigl* [2002] for a summary).

[29] We also compare EHB depths with the maximum depth determined using InSAR. Figure 10 shows that there is a good agreement between maximum earthquake depths determined using InSAR and EHB depths; the differences are normally distributed around zero with a standard deviation of about 10 km.
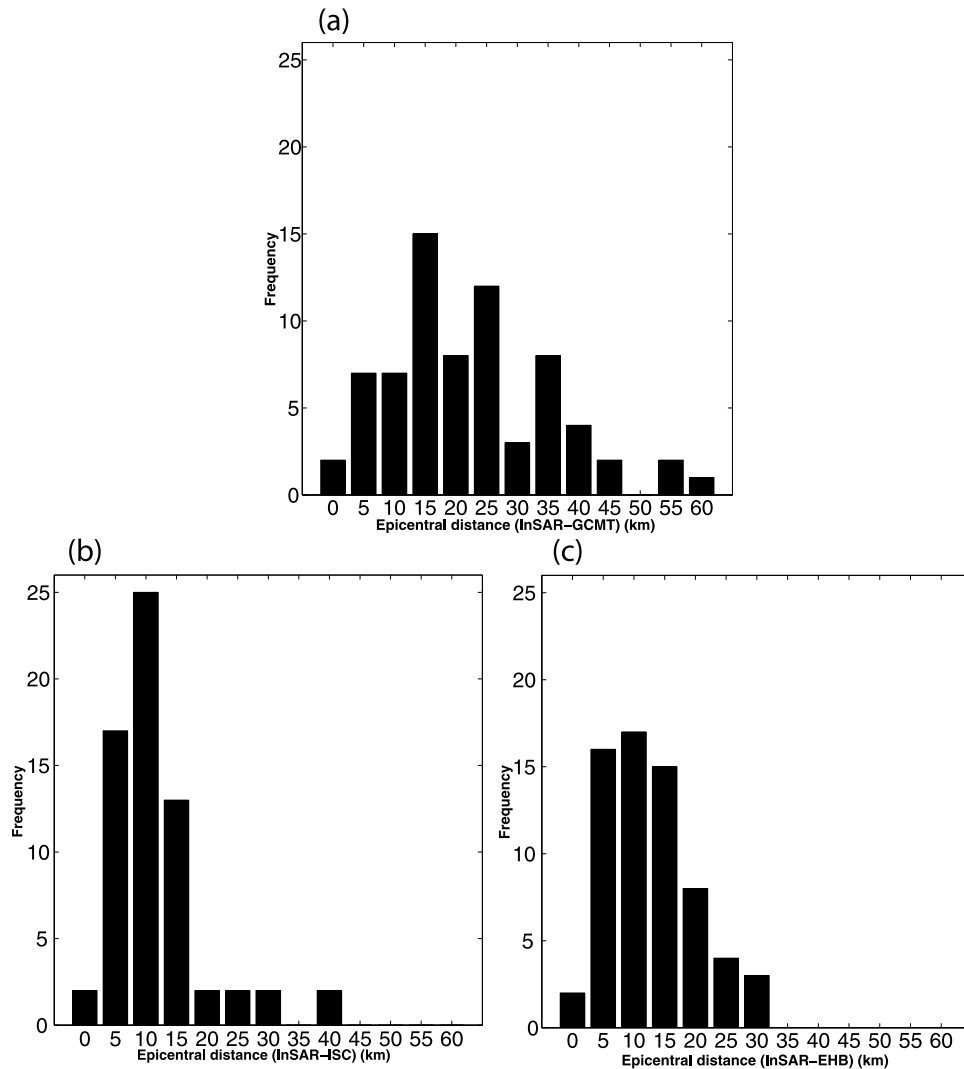
Figure 6. (a) Distribution of differences in epicentral location between 71 InSAR solutions and Global CMT determinations. The median and standard deviation of the distribution are 21.0 and 12.9 km, respectively. (b) Same as Figure 5a but for the ISC seismic catalog, for 65 epicentral distances determined using InSAR. Median is 9.3 km, and σ = 7.7 km. (c) Same as Figure 5b but for the EHB seismic catalog. Median is 11.4 km, and σ = 7.0 km.

[30] We observe a trend of increasing differences between InSAR and EHB depths as the moment magnitude increases (see Figure S8a). Moreover, depth differences also increase as the EHB depth increases (see Figure S8d). Finally, we do not observe any relationship between differences in InSAR and EHB depths and other parameters such as type of data used in the InSAR modeling, type of fault mechanism, earthquake non-double-couple component and postseismic time elapsed (see Figure S8, which shows these comparisons).

5. Discussion

[31] Some early studies of earthquake deformation using InSAR noted that the InSAR-derived seismic moment was larger than that estimated seismically [e.g., *Feigl et al.*, 1995; *Wright et al.*, 1999]. The compiled data set of InSAR-derived earthquake source parameters gives us the opportunity to test whether this reflects a true tendency in the results of InSAR data inversions, as suggested, e.g., by *Feigl* [2002], who considered also geodetic models without InSAR, or whether these are isolated observations. In this study we find that overall there are relatively small differences between InSAR and GCMT seismic moments, with a large standard deviation. We do not find a bias of InSAR estimating larger moment magnitudes than seismic data, and, if any, the only apparent tendency is that the differences between InSAR and GCMT seismic moment seem to be slightly skewed toward InSAR predicting smaller seismic moments than the GCMT. However, there are various factors that may affect our results, such as the nonhomogeneity of our compilation of InSAR source models resulting from the fact that they are generally obtained using different data sets and modeling tools, and our imperfect knowledge of rigidity (see section 2). Thus, our comparisons are affected by epistemic uncertainties and future work should be dedicated toward a better understanding and
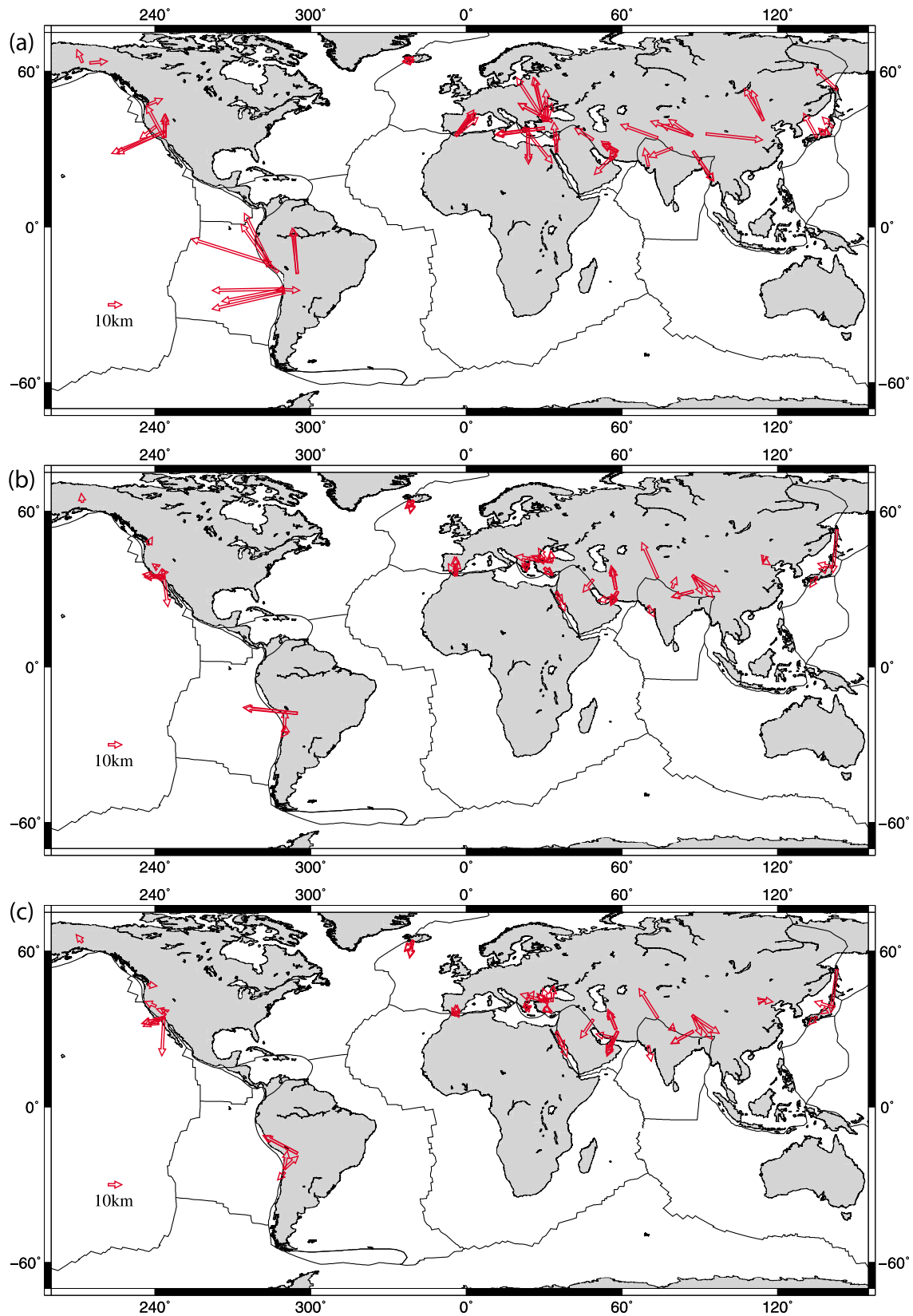
Figure 7. (a) Mislocation arrows between centroid epicentral locations in the GCMT catalog and those determined in 71 InSAR studies. The starting arrow point corresponds to the InSAR location. (b) Same as Figure 7a but for the ISC seismic catalog, for 65 epicentral locations determined using InSAR. (c) Same as Figure 7b but for the EHB seismic catalog. Note the arrow scale to the left in each diagram, which corresponds to 10 km.
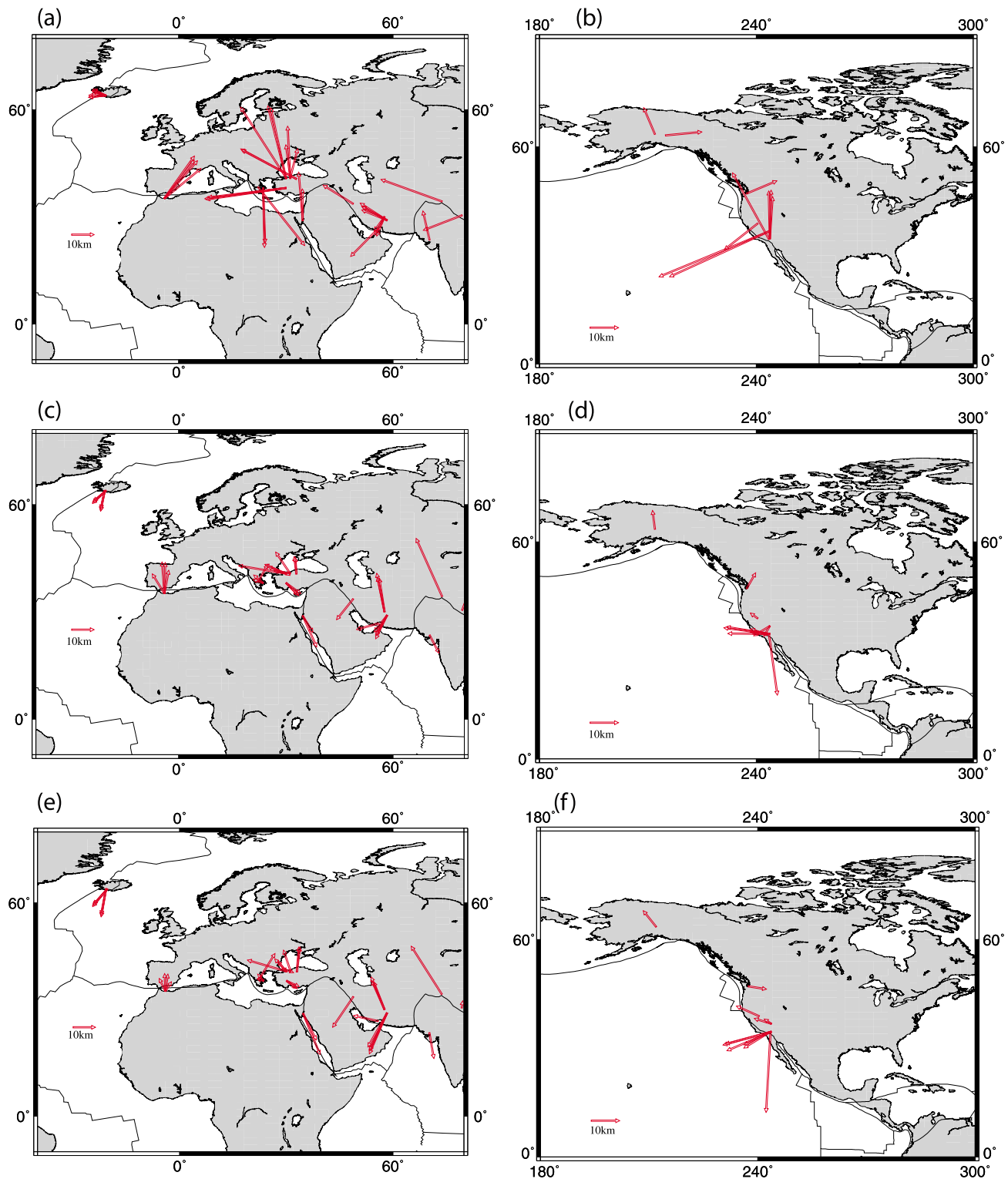
Figure 8. Mislocation arrows in (a, c, and e) North Africa, Europe and Middle East and (b, d, and f) North America between InSAR epicenters and GCMT (Figures 8a and 8b), ISC (Figures 8c and 8d), and EHB (Figures 8e and 8f) epicenters.

reduction of these uncertainties. In particular, it will be interesting to further investigate the trends found in this study using future compilations of InSAR CMT parameters ideally obtained using the same modeling techniques and using the same elastic moduli as in the seismic velocity models used to constrain the GCMT parameters. This will hopefully reduce not only differences between independent InSAR and seismic moment estimates, but also differences from distinct InSAR studies for a given earthquake, which can reach as much as 44% (see section 3.1). Moreover, it will also be interesting to
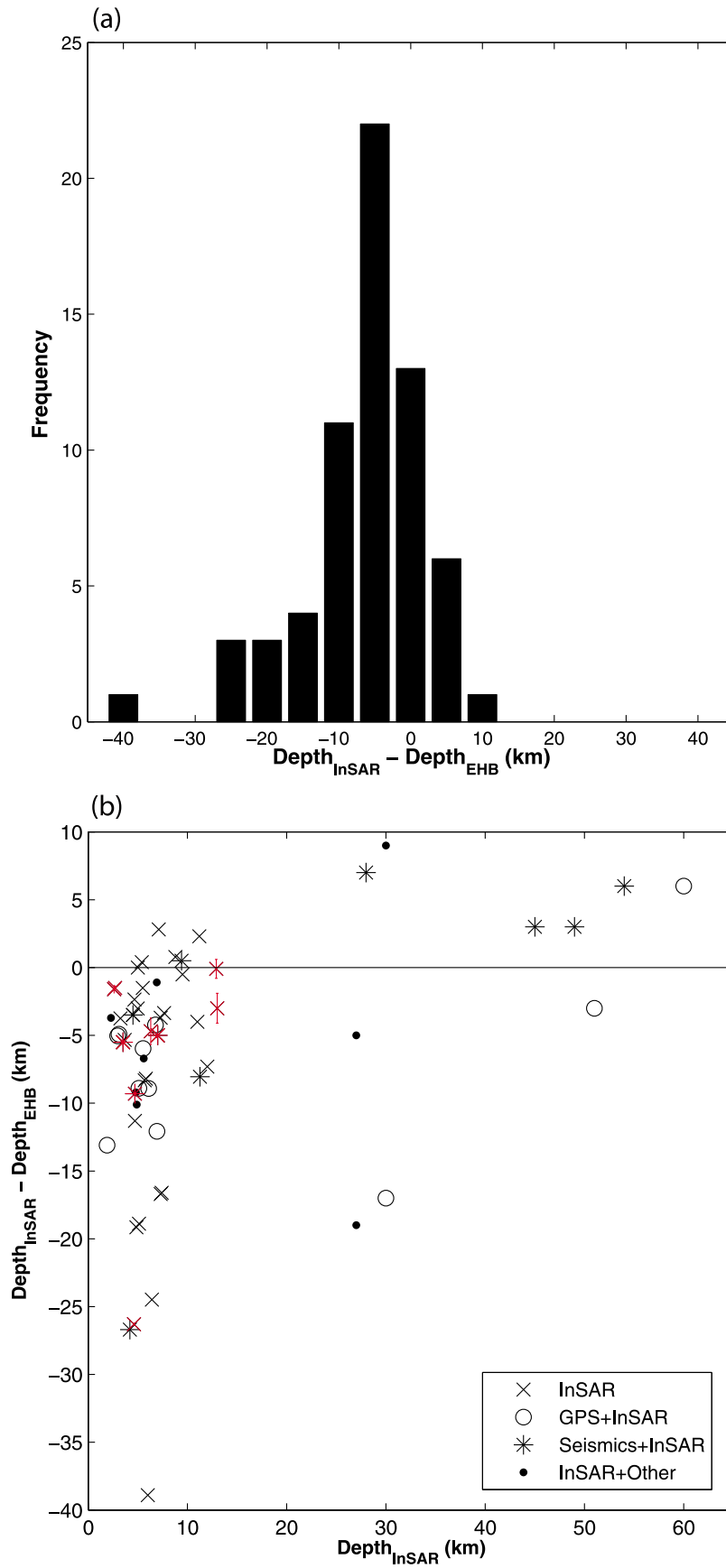
Figure 9
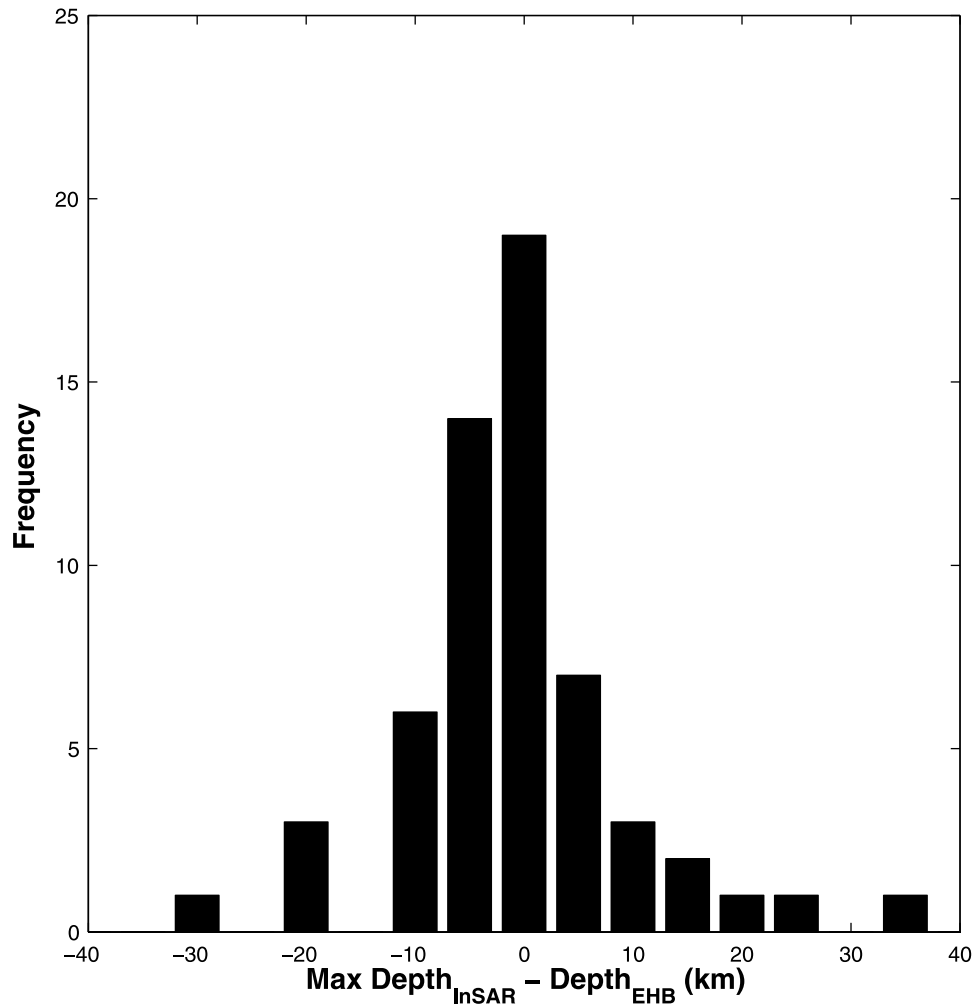
Figure 10. Distribution of the difference between EHB depth and 58 maximum depth values reported in InSAR studies published in the literature. The median and standard deviation of the distribution are −2.0 and 10.3 km, respectively.

carry out independent tests of the disagreeing source models, for example, by forward modeling.

[32] This study shows that overall there is a good agreement between fault strike, dip and rake determined using InSAR and GCMT for the earthquakes studied. The distribution of differences in strike shows the smallest spread, which is consistent with the fact that for shallow, large earthquakes, fault strike is in principle easier to constrain by the GCMT technique than dip and rake [*Dziewonski et al.*, 1981]; moreover, given the good spatial resolution of InSAR, strike determinations using InSAR data should also be quite accurate. Differences in fault rake between InSAR and GCMT show a wider distribution, which is probably due to limitations in both the GCMT method and in InSAR determinations, for which the quality of the rake estimate depends primarily on whether both ascending and des-

cending data are used [e.g., *Wright et al.*, 2004b]. Nevertheless, overall there is still a reasonable agreement in fault rake. These findings are consistent with the relatively small variability that we found in fault strike, dip and rake values obtained from different InSAR studies for a given earthquake (see section 3.1), suggesting that InSAR constrains these parameters well.

[33] Differences in epicentral location are larger when comparing InSAR with GCMT locations (median distance ~21 km), than for the ISC (median distance ~9 km) and EHB seismic catalogs (median distance ~11 km). These results are somewhat surprising, because, as for the InSAR solutions used in this study, the GCMT procedure determines the centroid location, whereas the ISC and EHB determine the earthquake's nucleation point using high-frequency first seismic arrivals. Since InSAR data have a

Figure 9. (a) Distribution of the difference in centroid depth between InSAR and EHB determinations for earthquakes investigated using 64 InSAR values published in the literature. The median and standard deviation of the distribution are −4.7 km and 8.7 km, respectively. (b) Differences in centroid depth between InSAR and EHB as a function of depth. The errors in depth estimated in some InSAR studies are taken into account and shown in red.

fine spatial resolution, which was confirmed by the very small variabilities in location for a given earthquake seen in section 3, it should map fault locations accurately. Thus, the epicentral differences found in this study indicate that the epicentral locations in the ISC and EHB catalogs are more accurate than those in the Global CMT catalog, even though in principle GCMT locations should be more comparable with InSAR centroid locations. InSAR epicentral shift vectors relative to seismic estimates are systematic in some regions (e.g., in Chile, Morocco, Greece and Turkey), but show no geographic consistency in other regions, such as in Iran and in California, suggesting a lack of epicentral resolution in some of the seismological estimates used in this study. The epicentral location errors that we estimate for the EHB and ISC catalogs are slightly smaller than the error in hypocentral locations determined by *Smith and Ekström* [1996], who obtain a RMS misfit to known locations close to 15 km when using corrections for three-dimensional Earth structure in inversions of high-frequency body wave traveltimes. Nevertheless, the EHB and ISC locations still seem to be less accurate than regional locations, whose errors are estimated by *Ritzwoller et al.* [2003] to be of about 5 km when using 3-D Earth models.

[34] As reported in previous studies, InSAR centroid depths are systematically shallower than the depths reported in the EHB catalog, with a median discrepancy of about 5 km. A tendency of geodetic estimates locating coseismic slip at shallower depths than seismological determinations has also been reported, e.g., by *Feigl* [2002]. A possible reason for this tendency is that the lower sensitivity of surface deformation to deep slip could bias the earthquake slip inferred by InSAR toward shallow depths. This is consistent with the fact that differences between InSAR and EHB depths are larger for greater EHB depths (see section 4.3.2). Several studies have highlighted that depths estimated using InSAR can be biased toward shallow values due to the use of elastic homogeneous half-spaces to model the InSAR data [e.g., *Savage*, 1987; *Marshall et al.*, 1991; *Eberhart-Phillips and Stuart*, 1992; *Wald and Graves*, 2001]. There are large variations in the properties of the upper crust and therefore such homogeneous half-space approximations will have the largest influence for shallow earthquakes, which constitute most of the earthquakes in our database. Quantifications of this effect using more realistic media such as layered 1-D and 3-D media, showed that using elastic homogeneous half-spaces in the modeling could lead to depths 10–30% shallower than the actual depth [e.g., *Marshall et al.*, 1991; *Savage*, 1998; *Lohman and Simons*, 2005; *Simons et al.*, 2002; *Bustin et al.*, 2004]. Comparing InSAR depth values in our database for earthquakes studied using both half-space and layered models, we observe depth differences in this same range, except for the 1995 Antofagasta earthquake, for which the depth in the layered model is actually shallower than for a half-space (see Table 1). Our ICMT database includes a total of nine InSAR earthquake models with reported depth obtained using layered media in the modeling (these models are indicated in italic in Tables 1–3). The median difference for these depths compared to EHB depths is of 2.6 km, i.e., for layered models, the InSAR depths are actually overall larger than the EHB depths, suggesting that indeed the use of half-space models could at least partly explain the depth dis-

crepancies. However, this needs to be further investigated, since our ICMT compilation contains a very small number of InSAR solutions determined using a layered model.

[35] Other possible reasons for the observed differences in depth include the use of incorrect rigidity and/or Poisson's ratio values [e.g., *Cattin et al.*, 1999], nonplanar fault geometries, irregular distribution of InSAR data or unmodeled rheological heterogeneity. Yet another possible cause for the trend observed in this study is that we compare InSAR estimates of centroid depth with depths reported in the EHB catalog, which are rupture initiation depths. It has been observed that the rupture of most shallow crustal earthquakes tends to propagate upward from a given depth toward the surface [e.g., *Mai et al.*, 2005], which is compatible with our observed tendency of the earthquake's centroid being systematically shallower than the rupture's initiation point, with a relatively small median of differences of about 5 km. Such small median of depth differences is reasonable, as most of the earthquakes used have magnitudes in the range M_w 6–6.5. The explanation of the observed trend in terms of upward propagation of the rupture is further supported by the good agreement that we obtain between EHB depths and maximum depths determined using InSAR (see Figure 10). Moreover, this explanation is also consistent with our observation that differences between InSAR and EHB depths are larger for greater moment magnitude earthquakes (see section 4.3.2). Thus, systematic differences between rupture initiation point and centroid for crustal earthquakes do seem to be a plausible explanation for the differences in depth that we observe, suggesting that the EHB and InSAR depths are both accurate within about 5 km.

6. Conclusions

[36] In this study we compare CMT source parameters determined using InSAR with those in the Global CMT, ISC and EHB seismic catalogs for 57 global earthquakes. We show that fault strike, dip and rake angles determined using InSAR are generally compatible with those in the Global CMT catalog. The comparisons suggest that at least for continental, moderate magnitude earthquakes that can be studied using InSAR, estimates of fault geometry and mechanism in the GCMT catalog and using InSAR data are accurate within about 15° in fault strike, dip and rake. We also show that the seismic moments determined using InSAR and seismic data are on average compatible with each other, with a standard deviation in moment magnitude of about 0.1. Moreover, we do not find support for previously suggested tendencies of InSAR data producing larger seismic moments than seismic data. We show that the median difference of GCMT epicentral locations relative to InSAR is of about 21 km, with a spread of 13 km, which reduces to half when using EHB and ISC locations. Since InSAR data have a high spatial resolution and are a new, independent data source, these comparisons constitute a first independent assessment of the epicentral location uncertainties in the GCMT, EHB and ISC catalogs. They suggest that the locations in the GCMT catalog can be improved, possibly by the use of future, high-resolution models of 3-D Earth structure; this issue deserves further investigation. Finally, we show that InSAR depths are biased by about 5 km

to shallower depths compared to EHB depths. This may be due to unmodeled local crustal structure and to the fact that while the InSAR solutions used here should represent the centroid of fault slip, the EHB method determines the earthquake's nucleation point. The latter explanation is consistent with the observation that shallow crustal earthquakes tend to propagate upward in the seismogenic layer. While in this study we focus on 57 earthquakes that occurred between 1992 and 2007, we are currently expanding our ICMT database by including InSAR source models that occurred since 2007 and will make it available to the wide community in the near future, thus contributing to current earthquake source model validation efforts. Moreover, we anticipate that this database will also form the basis for future comparisons of other relevant parameters, such as average slip and stress drop.

References

Adams, R. D., A. A. Hughes, and D. M. McGregor (1982), Analysis procedures at the International Seismological Centre, *Phys. Earth Planet. Inter.*, *30*, 85–93, doi:10.1016/0031-9201(82)90093-0.

Akoglu, A. M., Z. Cakir, M. Meghraoui, S. Belabbés, S. O. El Alami, S. Ergintav, and H. S. Akyuz (2006), The 1994–2004 Al Hoceima (Morocco) earthquake sequence: Conjugate fault ruptures deduced from InSAR, *Earth Planet. Sci. Lett.*, *252*, 467–480, doi:10.1016/j.epsl.2006.10.010.

Amelung, F., and J. W. Bell (2003), Double Spring Flat, Nevada, earthquake (M5.9): Main shock accompanied by triggered slip on a conjugate fault, *J. Geophys. Res.*, *108*(B9), 2433, doi:10.1029/2002JB001953.

Baer, G., G. J. Gunning, G. Shamir, and T. J. Wright (2008), The 1995 November 22, Mw 7.2 Gulf of Elat earthquake cycle revisited, *Geophys. J. Int.*, *175*, 1040–1054, doi:10.1111/j.1365-246X.2008.03901.x.

Belabbés, S., C. Wicks, Z. Cakir, and M. Meghraoui (2009), Rupture parameters of the 2003 Zemmouri (Mw 6.8), Algeria, earthquake from joint inversion of interferometric synthetic aperture radar, coastal uplift, and GPS, *J. Geophys. Res.*, *114*, B03406, doi:10.1029/2008JB005912.

Berberian, M., J. A. Jackson, E. Fielding, B. E. Parsons, K. Priestley, M. Qorashi, M. Tabelian, R. Walker, T. J. Wright, and C. Baker (2001), The 1998 March 14 Fandoqa earthquake (M_w 6.6) in Kerman province, southeast Iran: Re-rupture of the 1981 Sirch earthquake fault, triggering of slip on adjacent thrusts and the active tectonics of the Gowk fault zone, *Geophys. J. Int.*, *146*, 371–398, doi:10.1046/j.1365-246x.2001.01459.x.

Bernard, P., et al. (1997), The Ms = 6.2, June 15, 1995 Aigion earthquake (Greece): evidence for low angle normal faulting in the Corinth rift, *J. Seismol.*, *1*, 131–150, doi:10.1023/A:1009795618839.

Biggs, J., E. Bergman, B. Emmerson, G. J. Funning, J. Jackson, B. Parsons, and T. J. Wright (2006), Fault identification for buried strike-slip earthquakes using InSAR: The 1994 and 2004 Al Hoceima, Morocco earthquakes, *Geophys. J. Int.*, *166*, 1347–1362, doi:10.1111/j.1365-246X.2006.03071.x.

Burgmann, R., M. Emin Ayhan, E. J. Fielding, T. J. Wright, S. McClusky, B. Aktug, C. Demir, O. Lenk, and A. Turkezer (2002), Deformation during the 12 November 1999 Duzce, Turkey earthquake, from GPS and InSAR data, *Bull. Seismol. Soc. Am.*, *92*, 161–171, doi:10.1785/0120000834.

Bustin, A., R. D. Hyndman, A. Lambert, J. Ristau, J. He, H. Dragert, and M. Van der Kooij (2004), Fault parameters of the Nisqually earthquake

determined from moment tensor solutions and the surface deformation from GPS and InSAR, *Bull. Seismol. Soc. Am.*, *94*, 363–376, doi:10.1785/0120030073.

Cakir, Z., and A. M. Akoglu (2008), Synthetic aperture radar interferometry observations of the M = 6.0 Orta earthquake of 6 June 2000 (NW Turkey): Reactivation of a listric fault, *Geochem. Geophys. Geosyst.*, *9*, Q08009, doi:10.1029/2008GC002031.

Cakir, Z., J.-B. de Chabalier, R. Armijo, B. Meyer, A. Barka, and G. Peltzer (2003), Coseismic and early post-seismic slip associated with the 1999 Izmit earthquake (Turkey), from SAR interferometry and tectonic field observations, *Geophys. J. Int.*, *155*, 93–110, doi:10.1046/j.1365-246X.2003.02001.x.

Cakir, Z., M. Meghraoui, A. M. Akoglu, N. Jabour, S. Belabbes, and L. Ait-Brahim (2006), Surface deformation associated with the Mw 6.4, 24 February 2004 Al Hoceima, Morocco, earthquake deduced from InSAR: Implications for the active tectonics along North Africa, *Bull. Seismol. Soc. Am.*, *96*, 59–68, doi:10.1785/0120050108.

Cattin, R., P. Briole, H. Lyon-Caen, P. Bernard, and P. Pinettes (1999), Effects of superficial layers on coseismic displacements for a dip-slip fault and geophysical implications, *Geophys. J. Int.*, *137*, 149–158, doi:10.1046/j.1365-246x.1999.00779.x.

Dawson, J., P. Cummins, P. Tregoning, and M. Leonard (2008), Shallow intraplate earthquakes in western Australia observed by InSAR, *J. Geophys. Res.*, *113*, B11408, doi:10.1029/2008JB005807.

Delouis, B., P. Lundgren, J. Salichon, and D. Giardini (2000), Joint inversion of InSAR and teleseismic data for the slip history of the 1999 Izmit (Turkey) earthquake, *Geophys. Res. Lett.*, *27*, 3389–3392, doi:10.1029/2000GL011511.

Delouis, B., D. Giardini, P. Lundgren, and J. Salichon (2002), Joint inversion of InSAR, GPS, Teleseismic, and Strong-Motion data for the spatial and temporal distribution of earthquake slip: application to the 1999 Izmit aftershock, *Bull. Seismol. Soc. Am.*, *92*, 278–299, doi:10.1785/0120000806.

Dziewonski, A. M., and J. H. Woodhouse (1983a), Studies of the seismic source using normal-mode theory, *Proc. Enrico Fermi Int. Sch. Phys.*, *LXXXV*, 45–137.

Dziewonski, A. M., and J. H. Woodhouse (1983b), An experiment in systematic study of global seismicity: Centroid moment tensor solution for 201 moderate and large earthquakes of 1981, *J. Geophys. Res.*, *88*, 3247–3271, doi:10.1029/JB088iB04p03247.

Dziewonski, A. M., T.-A. Chou, and J. H. Woodhouse (1981), Determination of earthquake source parameters from waveform data for studies of global and regional seismicity, *J. Geophys. Res.*, *86*, 2825–2852, doi:10.1029/JB086iB04p02825.

Eberhart-Phillips, D., and W. D. Stuart (1992), Material heterogeneity simplifies the picture: Loma Prieta, *Bull. Seismol. Soc. Am.*, *82*(4), 1964–1968.

Engdahl, E. R., R. van der Hilst, and R. Buland (1998), Global teleseismic earthquake relocation with improved travel times and procedures for depth determination, *Bull. Seismol. Soc. Am.*, *88*, 722–743.

Feigl, K. L. (2002), Estimating earthquake source parameters from geodetic measurements, in *International Handbook of Earthquake and Engineering Seismology*, *Int. Geophys. Ser.*, vol. 81A, edited by W. H. K. Lee et al., pp. 607–620, Academic, Amsterdam, doi:10.1016/S0074-6142(02)80240-6.

Feigl, K. L., and C. H. Thurber (2009), A method for modelling radar interferograms without phase unwrapping: application to the M 5 Fawnskin, California earthquake of 1992 December 4, *Geophys. J. Int.*, *176*, 491–504, doi:10.1111/j.1365-246X.2008.03881.x.

Feigl, K. L., A. Sergent, and D. Jacq (1995), Estimation of an earthquake focal mechanism from a satellite radar interferogram: Application to the December 4, 1992 Landers aftershock, *Geophys. Res. Lett.*, *22*, 1037–1040, doi:10.1029/94GL03212.

Feigl, K. L., F. Sarti, H. Vadon, Mc, S. Ergintav, P. Durand, R. Burgmann, A. Rigo, D. Massonnet, and R. Reilinger (2002), Estimating slip distribution for the Izmit mainshock from coseismic GPS, ERS-1, RADARSAT, and SPOT measurements, *Bull. Seismol. Soc. Am.*, *92*, 138–160, doi:10.1785/0120000830.

Ferreira, A. M. G., J. Weston, and G. J. Funning (2011), Global compilation of interferometric synthetic aperture earthquake source models: 2. Effects of 3-D Earth structure, *J. Geophys. Res.*, doi:10.1029/2010JB008132, in press.

Fialko, Y. (2004), Probing the mechanical properties of seismically active crust with space geodesy: Study of the coseismic deformation due to the 1992 Mw7.3 Landers (southern California) earthquake, *J. Geophys. Res.*, *109*, B03307, doi:10.1029/2003JB002756.

Fujiwara, S., H. Yarai, S. Ozawa, M. Tobita, M. Murakami, H. Nakagawa, and K. Nitta (1998), Surface displacement of the March 26, 1997 Kagoshima-ken Hokuseibu earthquake in Japan from synthetic aperture radar interferometry, *Geophys. Res. Lett.*, *25*, 4541–4544, doi:10.1029/1998GL900191.

Fukahata, Y., and T. J. Wright (2008), A non-linear geodetic data inversion using ABIC for slip distribution on a fault with an unknown dip angle, *Geophys. J. Int.*, 173, 353–364, doi:10.1111/j.1365-246X.2007.03713.x.

Fukushima, Y., T. Ozawa, and M. Hashimoto (2008), Fault model of the 2007 Noto Hanto earthquake estimated from PALSAR radar interferometry and GPS data, *Earth Planets Space*, 60, 99–104.

Funning, G. J. (2005), Source parameters of large shallow earthquakes in the Alpine-Himalayan belt from InSAR and waveform modelling, Ph.D. thesis, Fac. of Phys. Sci., Univ. of Oxford., Oxford, U. K.

Funning, G. J., B. Parsons, T. J. Wright, J. A. Jackson, and E. J. Fielding (2005a), Surface displacements and source parameters of the 2003 Bam (Iran) earthquake from Envisat advanced synthetic aperture radar imagery, *J. Geophys. Res.*, 110, B09406, doi:10.1029/2004JB003338.

Funning, G. J., R. M. D. Barker, S. H. Lamb, E. Minaya, B. Parsons, and T. J. Wright (2005b), The 1998 Aiquile, Bolivia earthquake: A seismically active fault revealed with InSAR, *Earth Planet. Sci. Lett.*, 232, 39–49, doi:10.1016/j.epsl.2005.01.013.

Funning, G. J., B. Parsons, and T. J. Wright (2007), Fault slip in the 1997 Manyi, Tibet earthquake from linear elastic modelling of InSAR displacements, *Geophys. J. Int.*, 169, 988–1008, doi:10.1111/j.1365-246X.2006.03318.x.

Jonsson, S., H. Zebker, P. Segall, and F. Amelung (2002), Fault slip distribution of the 1999 Mw 7.1 Hector Mine, California, earthquake, estimated from satellite radar and GPS measurements, *Bull. Seismol. Soc. Am.*, 92, 1377–1389, doi:10.1785/0120000922.

Klinger, Y., R. Michel, and J.-P. Avouac (2000), Co-seismic deformation during the Mw 7.3 Aqaba earthquake (1995) from ERS-SAR interferometry, *Geophys. Res. Lett.*, 27, 3651–3654, doi:10.1029/1999GL008463.

Kontoes, C., P. Elias, O. Sykioti, P. Briole, D. Remy, M. Sachpazi, I. Veis, and G. Kotsis (2000), Displacement field and fault model for the September 7, 1999 Athens earthquake inferred from ERS2 satellite radar interferometry, *Geophys. Res. Lett.*, 27, 3989–3992, doi:10.1029/2000GL008510.

Lasserre, C., G. Peltzer, F. Crampé, Y. Klinger, J. Van der Woerd, and P. Tapponnier (2005), Coseismic deformation of the 2001 Mw = 7.8 Kokoxili earthquake in Tibet, measured by synthetic aperture radar interferometry, *J. Geophys. Res.*, 110, B12408, doi:10.1029/2004JB003500.

Li, Z., W. Feng, Z. Xu, P. Cross, and J. Zhang (2008), 1998 Mw 5.7 Zhangbei-Shangyi (China) earthquake revisited: A buried thrust fault revealed with interferometric synthetic aperture radar, *Geochem. Geophys. Geosyst.*, 9, Q04026, doi:10.1029/2007GC001910.

Lohman, R. B., and M. Simons (2005), Locations of selected small earthquakes in the Zagros mountains, *Geochem. Geophys. Geosyst.*, 6, Q03001, doi:10.1029/2004GC000849.

Lohman, R. B., M. Simons, and B. Savage (2002), Location and mechanism of the Little Skull Mountain earthquake as constrained by satellite radar interferometry and seismic waveform modeling, *J. Geophys. Res.*, 107(B6), 2118, doi:10.1029/2001JB000627.

Mai, P. M., P. Spudich, and J. Boatwright (2005), Hypocenter locations in finite-source rupture models, *Bull. Seismol. Soc. Am.*, 95(3), 965–980, doi:10.1785/0120040111.

Marshall, G. A., R. S. Stein, and W. Thatcher (1991), Faulting geometry and slip from coseismic elevation changes: The 18 October 1989, Loma Prieta, California, earthquake, *Bull. Seismol. Soc. Am.*, 81, 1660–1693.

Massonnet, D., and K. L. Feigl (1995), Satellite radar interferometric map of the coseismic deformation field of the M = 6.1 Eureka Valley, California earthquake of May 17, 1993, *Geophys. Res. Lett.*, 22, 1541–1544, doi:10.1029/95GL01088.

Massonnet, D., K. L. Feigl, H. Vadon, and M. Rossi (1994), Radar interferometric mapping of deformation in the year after the Landers earthquake, *Nature*, 369, 227–230, doi:10.1038/369227a0.

Massonnet, D., K. L. Feigl, H. Vadon, and M. Rossi (1996), Coseismic deformation field of the M = 6.7 Northridge California earthquake of January 17, 1994 recorded by two radar satellites using interferometry, *Geophys. Res. Lett.*, 23, 969–972, doi:10.1029/96GL00729.

Meyer, B., R. Armijo, D. Massonnet, J.-B. de Chabalier, C. Delacourt, J. C. Ruegg, J. Achache, P. Briole, and D. Papanastassiou (1996), The 1995 Grevena (northern Greece) earthquake: Fault model constrained with tectonic observations and SAR interferometry, *Geophys. Res. Lett.*, 23, 2677–2680, doi:10.1029/96GL02389.

Motagh, M., J. Klotz, F. Tavakoli, Y. Djamour, S. Arabi, H.-U. Wetzel, and J. Zschau (2006), Combination of precise leveling and InSAR data to constrain source parameters of the Mw = 6.5, 26 December 2003 Bam, earthquake, *Pure Appl. Geophys.*, 163, 1–18, doi:10.1007/s00024-005-0005-y.

Nishimura, S., S. Fujiwara, M. Murakami, H. Suito, M. Tobita, and H. Yarai (2006), Fault model of the 2005 Fukuoka-ken Seiho-oki earthquake estimated from coseismic deformation observed by GPS and InSAR, *Earth Planets Space*, 58, 51–56.

Nishimura, T., S. Fujiwara, M. Murakami, M. Tobita, H. Nakagawa, T. Sagiya, and T. Tada (2001), The M6.1 earthquake triggered by volcanic inflation of Iwate volcano, northern Japan, observed by satellite radar interferometry, *Geophys. Res. Lett.*, 28, 635–638, doi:10.1029/2000GL012022.

Nishimura, T., T. Imakiire, H. Yarai, T. Ozawa, M. Murakami, and M. Kaidzu (2003), A preliminary fault model of the 2003 July 26, M6.4 northern Miyagi earthquake, northeastern Japan, estimated from joint inversion of GPS leveling and InSAR data, *Earth Planets Space*, 55, 751–757.

Nissen, E., M. Ghorashi, J. Jackson, B. Parsons, and M. Talebian (2007), The 2005 Qeshm island earthquake (Iran)—A link between buried reverse faulting and surface folding in the Zagros simply folded belt, *Geophys. J. Int.*, 171, 326–338, doi:10.1111/j.1365-246X.2007.03514.x.

Ozawa, S., M. Murakami, S. Fujiwara, and M. Tobita (1997), Synthetic aperture radar interferogram of the 1995 Kobe earthquake and its geodetic inversion, *Geophys. Res. Lett.*, 24, 2327–2330, doi:10.1029/97GL02318.

Ozawa, S., H. Yarai, M. Tobita, H. Une, and T. Nishimura (2008), Crustal deformation associated with the Noto Hanto earthquake in 2007 in Japan, *Earth Planets Space*, 60, 95–98.

Ozawa, T., S. Nishimura, Y. Wada, and H. Ohkura (2005), Coseismic deformation of the Mid Niigata prefecture earthquake in 2004 detected by RADARSAT/InSAR, *Earth Planets Space*, 57, 423–428.

Pathier, E., E. J. Fielding, T. J. Wright, R. Walker, B. E. Parsons, and S. Hensley (2006), Displacement field and slip distribution of the 2005 Kashmir earthquake from SAR imagery, *Geophys. Res. Lett.*, 33, L20310, doi:10.1029/2006GL027193.

Pedersen, R., F. Sigmundsson, K. L. Feigl, and T. Arnadottir (2001), Coseismic interferograms of two Ms = 6.6 earthquakes in the south Iceland seismic zone, June 2000, *Geophys. Res. Lett.*, 28, 3341–3344, doi:10.1029/2001GL013235.

Pedersen, R., S. Jonsson, T. Arnadottir, F. Sigmundsson, and K. L. Feigl (2003), Fault slip distribution of two June 2000 Mw6.5 earthquakes in south Iceland estimated from joint inversion of InSAR and GPS measurements, *Earth Planet. Sci. Lett.*, 213, 487–502, doi:10.1016/S0012-821X(03)00302-9.

Peltzer, G., and P. Rosen (1995), Surface displacement of the 17 May 1993 Eureka Valley, California, earthquake observed by SAR interferometry, *Science*, 268, 1333–1336, doi:10.1126/science.268.5215.1333.

Peyrat, S., et al. (2006), Tarapaca intermediate-depth earthquake (Mw 7.7, 2005, northern Chile): A slab-pull event with horizontal fault plane constrained from seismologic and geodetic observations, *Geophys. Res. Lett.*, 33, L22308, doi:10.1029/2006GL027710.

Peyret, M., J. Chery, Y. Djamour, A. Avallone, F. Sarti, P. Briole, and M. Sarpoulaki (2007), The source motion of 2003 Bam (Iran) earthquake constrained by satellite and ground-based geodetic data, *Geophys. J. Int.*, 169, 849–865, doi:10.1111/j.1365-246X.2007.03358.x.

Peyret, M., F. Rolandone, S. Dominguez, Y. Djamour, and B. Meyer (2008), Source model for the Mw 6.1, 31 March 2006, Chalan-Chulan earthquake (Iran) from InSAR, *Terra Nova*, 20, 126–133, doi:10.1111/j.1365-3121.2008.00797.x.

Pritchard, M. E., and E. J. Fielding (2008), A study of the 2006 and 2007 earthquake sequence of Pisco, Peru, with InSAR and teleseismic data, *Geophys. Res. Lett.*, 35, L09308, doi:10.1029/2008GL033374.

Pritchard, M. E., M. Simons, P. A. Rosen, S. Hensley, and F. H. Webb (2002), Co-seismic slip from the 1995 July 30 Mw = 8.1 Antofagasta, Chile, earthquake as constrained by InSAR and GPS observations, *Geophys. J. Int.*, 150, 362–376, doi:10.1046/j.1365-246X.2002.01661.x.

Pritchard, M. E., C. Ji, and M. Simons (2006), Distribution of slip from 11 Mw ≥ 6 earthquakes in the northern Chile subduction zone, *J. Geophys. Res.*, 111, B10302, doi:10.1029/2005JB004013.

Pritchard, M. E., E. O. Norabuena, C. Ji, R. Boroschek, D. Comte, M. Simons, T. H. Dixon, and P. Rosen (2007), Geodetic, teleseismic, and strong motion constraints on slip from recent southern Peru subduction zone earthquakes, *J. Geophys. Res.*, 112, B03307, doi:10.1029/2006JB004294.

Resor, P. G., D. D. Pollard, T. J. Wright, and G. C. Beroza (2005), Integrating high-precision aftershock locations and geodetic observations to model coseismic deformation associated with the 1995 Kozani-Grevena earthquake, Greece, *J. Geophys. Res.*, 110, B09402, doi:10.1029/2004JB003263. (Correction to "Integrating high-precision aftershock locations and geodetic observations to model coseismic deformation associated with the 1995 Kozani-Grevena earthquake, Greece," *J. Geophys. Res.*, 112, B11402, doi:10.1029/2007JB005389, 2007.)

Rigo, A., J.-B. de Chabalier, B. Meyer, and R. Armijo (2004), The 1995 Kozani-Grevena (northern Greece) earthquake revisited: an improved faulting model from synthetic radar interferometry, *Geophys. J. Int.*, 157, 727–736, doi:10.1111/j.1365-246X.2004.02220.x.

Ritzwoller, M. H., N. M. Shapiro, A. L. Levshin, E. A. Bergman, and E. R. Engdahl (2003), Ability of a global three-dimensional model to locate

regional events, *J. Geophys. Res.*, *108*(B7), 2353, doi:10.1029/2002JB002167.

Salichon, J., B. Delouis, P. Lundgren, D. Giardini, M. Costantini, and P. Rosen (2003), Joint inversion of broadband teleseismic and interferometric synthetic aperture radar (InSAR) data for the slip history of the Mw = 7.7, Nazca ridge (Peru) earthquake of 12 November 1996, *J. Geophys. Res.*, *108*(B2), 2085, doi:10.1029/2001JB000913.

Salichon, J., P. Lundgren, B. Delouis, and D. Giardini (2004), Slip history of the 16 October 1999 Mw 7.1 Hector Mine earthquake (California) from the inversion of InSAR, GPS, and teleseismic data, *Bull. Seismol. Soc. Am.*, *94*, 2015–2027, doi:10.1785/0120030038.

Salvi, S., et al. (2000), Modeling coseismic displacements resulting from SAR interferometry and GPS measurements during the 1997 Umbria-Marche seismic sequence, *J. Seismol.*, *4*, 479–499, doi:10.1023/A:1026502803579.

Satyabala, S. P. (2006), Coseismic ground deformation due to an intraplate earthquake using synthetic aperture radar interferometry: The Mw6.1 Killari, India, earthquake of 29 September 1993, *J. Geophys. Res.*, *111*, B02302, doi:10.1029/2004JB003434.

Satyabala, S. P., and R. Bilham (2006), Surface deformation and subsurface slip of the 28 March 1999 Mw = 6.4 west Himalayan Chamoli earthquake from InSAR analysis, *Geophys. Res. Lett.*, *33*, L23305, doi:10.1029/2006GL027422.

Savage, J. C. (1987), Effect of crustal layering upon dislocation modeling, *J. Geophys. Res.*, *92*, 10,595–10,600, doi:10.1029/JB092iB10p10595.

Savage, J. C. (1998), Displacement field for an edge dislocation in a layered half-space, *J. Geophys. Res.*, *103*, 2439–2446, doi:10.1029/97JB02562.

Schmidt, D. A., and R. Burgmann (2006), InSAR constraints on the source parameters of the 2001 Bhuj earthquake, *Geophys. Res. Lett.*, *33*, L02315, doi:10.1029/2005GL025109.

Shamir, G., G. Baer, and A. Hofstetter (2003), Three-dimensional elastic earthquake modelling based on integrated seismological and InSAR data: The M_w = 7.2 Nuweiba earthquake, Gulf of Elat/Aqaba 1995 November, *Geophys. J. Int.*, *154*, 731–744, doi:10.1046/j.1365-246X.2003.01978.x.

Simons, M., Y. Fialko, and L. Rivera (2002), Coseismic deformation from the 1999 Mw7.1 Hector Mine, California, earthquake as inferred from InSAR and GPS observations, *Bull. Seismol. Soc. Am.*, *92*, 1390–1402, doi:10.1785/0120000933.

Smith, G., and G. Ekström (1996), Improving teleseismic event locations using a three-dimensional earth model, *Bull. Seismol. Soc. Am.*, *86*, 788–796.

Stich, D., F. de L. Mancilla, D. Baumont, and J. Morales (2005), Source analysis of the Mw 6.3 2004 Al Hoceima earthquake (Morocco) using regional apparent source time functions, *J. Geophys. Res.*, *110*, B06306, doi:10.1029/2004JB003366.

Stramondo, S., et al. (1999), The September 26, 1997 Colfiorito, Italy, earthquakes: Modelled coseismic surface displacement from SAR interferometry and GPS, *Geophys. Res. Lett.*, *26*, 883–886, doi:10.1029/1999GL900141.

Syracuse, E. M., and G. A. Abers (2009), Systematic biases in subduction zone hypocenters, *Geophys. Res. Lett.*, *36*, L10303, doi:10.1029/2009GL037487.

Tahayt, A., et al. (2009), The Al Hoceima (Morocco) earthquake of 24 February 2004, analysis and interpretation of data from ENVISAT ASAR and SPOT5 validated by ground-based observations, *Remote Sens. Environ.*, *113*, 306–316, doi:10.1016/j.rse.2008.09.015.

Talebian, M., et al. (2006), The Dahuiyeh (Zarand) earthquake of 2005 February 22 in central Iran: reactivation of an intramountain reverse fault, *Geophys. J. Int.*, *164*, 137–148, doi:10.1111/j.1365-246X.2005.02839.x.

Tobita, M., S. Fujiwara, S. Ozawa, P. A. Rosen, E. J. Fielding, C. L. Werner, M. Murakami, H. Nakagawa, K. Nitta, and M. Murakami (1998), Deformation of the 1995 North Sakhalin earthquake detected by jERS-1/SAR interferometry, *Earth Planets Space*, *50*, 313–325.

Wald, D. J., and R. W. Graves (2001), Resolution analysis of finite fault source inversion using one- and three-dimensional Green's functions: 2. Combining seismic and geodetic data, *J. Geophys. Res.*, *106*, 8767–8788, doi:10.1029/2000JB900435.

Wang, H., C. Xu, and L. Ge (2007), Coseismic deformation and slip distribution of the 1997 Mw7.5 Manyi, Tibet, earthquake from InSAR measurements, *J. Geodyn.*, *44*, 200–212, doi:10.1016/j.jog.2007.03.003.

Wright, T. J. (2000), Crustal deformation in Turkey from synthetic aperture radar interferometry, Ph.D. thesis, Fac. of Phys. Sci., Univ. of Oxford, Oxford, U. K.

Wright, T. J., B. E. Parsons, J. A. Jackson, M. Haynes, E. J. Fielding, P. C. England, and P. J. Clarke (1999), Source parameters of the 1 October 1995 Dinar (Turkey) earthquake from SAR interferometry and seismic body-wave modelling, *Earth Planet. Sci. Lett.*, *172*, 23–37, doi:10.1016/S0012-821X(99)00186-7.

Wright, T. J., Z. Lu, and C. Wicks (2003), Source model for the M w 6.7, 23 October 2002, Nenana Mountain earthquake (Alaska) from InSAR, *Geophys. Res. Lett.*, *30*(18), 1974, doi:10.1029/2003GL018014.

Wright, T. J., Z. Lu, and C. Wicks (2004a), Constraining the slip distribution and fault geometry of the Mw 7.9, 3 November 2002, Denali fault earthquake with interferometric synthetic aperture radar and global positioning system data, *Bull. Seismol. Soc. Am.*, *94*, S175–S189, doi:10.1785/0120040623.

Wright, T. J., B. E. Parsons, and Z. Lu (2004b), Toward mapping surface deformation in three dimensions using InSAR, *Geophys. Res. Lett.*, *31*, L01607, doi:10.1029/2003GL018827.

A. M. G. Ferreira and J. Weston, School of Environmental Sciences, University of East Anglia, Norwich NR4 7TJ, UK. (A.Ferreira@uea.ac.uk; J.Weston@uea.ac.uk)

G. J. Funning, Department of Earth Sciences, University of California, Riverside, CA 92521, USA. (gareth@ucr.edu)